Intra-slab COH fluid fluxes evidenced by fluid-mediated decarbonation of lawsonite eclogite-facies altered oceanic metabasalts

Dear author,

Please note that changes made in the online proofing system will be added to the article before publication but are not reflected in this PDF.

We also ask that this file not be used for submitting corrections.

Lithos xxx (2018) xxx–xxx

Contents lists available at ScienceDirect

Lithos

journal homepage: www.elsevier.com/locate/lithos

Intra-slab COH fluid fluxes evidenced by fluid-mediated decarbonation of lawsonite eclogite-facies altered oceanic metabasalts

Alberto Vitale Brovarone [a,*], Xu Chu [b,c], Laure Martin [d], Jay J. Ague [b], Patrick Monié [e], Chiara Groppo [f], Isabelle Martinez [g], Carine Chaduteau [g]

[a] Institut de Minéralogie et de Physique des Matériaux et de Cosmochimie, UMR 7590 CNRS-UPMC-IRD-MNHN, Campus Jussieu, Tour 23 - Couloir 13/23 - 4e étage - Bureau 05, Case courrier 115, 4 Place Jussieu, 75252 Paris Cedex 05, France
[b] Department of Geology and Geophysics, Yale University, P.O. Box 208109, New Haven, CT 06520, USA
[c] Department of Earth Sciences, University of Toronto, 22 Russell St., Toronto, ON M5S 3B1, Canada
[d] CCFS-CMCA, Arc Centre for Core to Crust Fluid Systems, Centre for Microscopy, Characterisation and Analysis, University of Western Australia, Crawley, WA 6009, Australia
[e] Geosciences Montpellier, UMR CNRS 5243, Université Montpellier 2, Montpellier, France
[f] Dipartimento di Scienze della Terra, Università degli Studi di Torino, and IGG-CNR, via Valperga Caluso 35, 10100 Torino, Italy
[g] Institut de Physique du Globe de Paris, Sorbonne Paris Cité, Université Paris Diderot, UMR 7154 CNRS, 1 rue Jussieu, F-75005 Paris, France

ARTICLE INFO

Article history:
Received 21 July 2017
Accepted 24 January 2018
Available online xxxx

Keywords:
C cycle
C fluxes at subduction zones
HP metamorphism
Subducted altered oceanic crust
Lawsonite-eclogites
Alpine Corsica

ABSTRACT

The interplay between the processes controlling the mobility of H_2O and C-bearing species during subduction zone metamorphism exerts a critical control on plate tectonics and global volatile recycling. Here we present the first study on fresh, carbonate-bearing, lawsonite eclogite-facies metabasalts from Alpine Corsica, France, which reached the critical depths at which important devolatilization reactions occur in subducting slabs. The studied samples indicate that the evolution of oceanic crustal sequences subducted under present-day thermal regimes is dominated by localized fluid-rock interactions that are strongly controlled by the nature and extent of inherited (sub)seafloor hydrothermal processes, and by the possibility of deep fluids to be channelized along inherited or newly-formed discontinuities. Fluid channelization along inherited discontinuities controlled local rehydration and dehydration/decarbonation reactions and the stability of carbonate and silicate minerals at the blueschist-eclogite transition. Fluid-mediated decarbonation was driven by upward, up-temperature fluid flow in the inverted geothermal gradient of a subducting oceanic slab, a process that has not been documented in natural samples to date. We estimate that the observed fluid-rock reactions released 20–60 kg CO_2 per m^3 of rock (i.e. ~0.7–2.1 wt% CO_2), which is in line with the values predicted from decarbonation of metabasalts in open systems at these depths. Conversely, the estimated time-integrated fluid fluxes (20–50 t/m^2) indicate that the amount of carbon transported by channelized fluid flow within the volcanic part of subducting oceanic plates is potentially much higher than previous numerical estimates, testifying to the percolation of C-bearing fluids resulting from devolatilization/dissolution processes operative in large reservoirs.

1. Introduction

Altered oceanic crust is a major carrier of C in subduction zones (dominantly as carbonate) (Staudigel, 2014), and its metamorphic evolution plays a critical role in controlling C fluxes to the deep mantle or back to shallow reservoirs, as indicated by several experimental (Hammouda, 2003; Poli et al., 2009; Keshav and Gudfinnsson, 2010; Poli, 2015), numerical (Kerrick and Connolly, 2001; Gorman et al., 2006; Collins et al., 2015) and field-based studies (Li et al., 2012, 2014; Collins et al., 2015).

The budget of carbonates at subduction zones depends on the interplay between processes producing carbonic fluids, such as decarbonation reactions, carbonate dissolution and melting, and those consuming carbon from the fluid in favor of carbonate precipitation, such as carbonation and veining. The role of decarbonation reactions (e.g. reactions between carbonates and silicates) on the carbonate budget of subduction zones has been extensively investigated by experimental and thermodynamic studies (Kerrick and Connolly, 2001; Gorman et al., 2006; Poli et al., 2009; Gonzalez et al., 2016). Carbonate dissolution (solubility of carbonate in a fluid at given pressure -P- and temperature -T-) has been only recently introduced to the common terminology of subduction-related processes (Frezzotti et al., 2011; Ague and Nicolescu, 2014; Facq et al., 2014; Kelemen and Manning, 2015; Ferrando et al., 2017), and has been shown to play a major role in the

* Corresponding author.
E-mail address: alberto.vitale-brovarone@impmc.upmc.fr (A.V. Brovarone).

https://doi.org/10.1016/j.lithos.2018.01.028
0024-4937/

production of carbonic fluids at forearc and subarc depths. Carbonate melting is also an important process controlling the stability of carbonates (Poli, 2015); it takes place at P-T conditions much higher than those considered in this study, so is not discussed further. The carbonic fluids produced by these processes may migrate towards shallower reservoirs (i.e. mantle wedge, volcanic arcs) (Kelemen and Manning 2015 for review), or reprecipitate as secondary carbonate in metamorphic veins or during carbonation of silicates in the slab at high-pressure (HP) conditions (Piccoli et al., 2016; Scambelluri et al., 2016).

All the above-mentioned processes are strongly enhanced by the infiltration of aqueous fluids in carbonate-bearing rocks (Gorman et al., 2006; Frezzotti et al., 2011; Ague and Nicolescu, 2014). The transition from blueschist- to eclogite-facies metamorphic conditions takes place in the forearc region of subduction zones (ca. 70–80 km), and has long been shown to be the locus of important dehydration reactions (e.g. breakdown of glaucophane and lawsonite in favor of omphacite and garnet) releasing considerable amounts of aqueous fluids (van Keken et al., 2011). The percolation of these fluids at eclogite-facies conditions within the slab may therefore enhance fluid-rock processes and modify the equilibria controlling the stability of carbonates as either solid or fluid phases (Gorman et al., 2006; Ague and Nicolescu, 2014; Gonzalez et al., 2016; Piccoli et al., 2016).

Natural HP rocks exhumed in mountain belts provide an important means to study how the interplay between different CO_2-producing and -consuming processes affects the carbonate budgets during subduction of oceanic crust at the critical depth of 70–80 km where large amounts of aqueous fluids are released. Moreover, natural samples provide information on the mechanisms of fluid-flow (e.g. pervasive vs. channelized), and on the structural/mineralogical control of geological media and their effects on devolatilization processes (Molina et al., 2004; Plümper et al., 2016). Natural examples featuring the role of fluid flushing on carbonate dissolution in slab-forming rocks are increasingly documented (Frezzotti et al., 2011; Ague and Nicolescu, 2014; Ferrando et al., 2017). Theoretical studies predict that also decarbonation reaction and significant CO_2 release may be induced by upward fluid infiltration at depths corresponding to the blueschist-eclogite transition (Gorman et al., 2006). However, most field-based petrological studies of HP/LT carbonate-bearing lithologies have focused on closed systems pointing to little decarbonation at these depths (Cook-Kollars et al., 2014; Collins et al., 2015). Field evidence for decarbonation of subducted rocks by upward, up-T fluid flow during eclogitization is lacking.

The goal of this study is to examine the interplay between oceanic structural inheritance and fluid-rock processes including dehydration, rehydration, decarbonation and carbonate dissolution, and their contributions to the fate of carbonates in subducted altered oceanic crust. Here we provide the first study of these processes on fresh lawsonite eclogite-facies carbonated metabasalts by integrating field, textural, geochemical and thermodynamic data from Alpine Corsica, together with observations from weakly metamorphosed equivalents. Corsica hosts exceptionally fresh lawsonite-bearing assemblages that are typically completely replaced by lower-P/higher-T, retrograde assemblages in most HP-LT orogenic belts. Moreover, the preservation of primary oceanic structures is widespread. Thus, Corsica represents a rare opportunity to study the pristine lawsonite eclogite-facies reactions driven by up-T fluid flow in a down-going oceanic slab at the critical zone (70–80 km depth) where important petrological processes are predicted for most past (since the Phanerozoic; Tsujimori and Ernst, 2014) and active subduction settings (Syracuse et al., 2010) (Fig. 1).

2. Geological setting

Corsica, France, is a part of the Alpine orogenic system now isolated from the European mainland by the opening of two Tertiary basins, namely the Ligurian-Provençal and the Tyrrhenian basins (Jolivet et al., 1998; Malavieille et al., 1998; Malusà et al., 2015) (Fig. 2). The

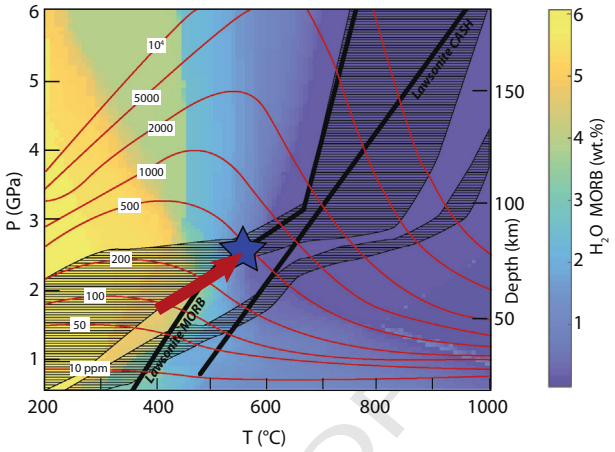

Fig. 1. P-T diagram showing the significance of the Corsican assemblages with respect to the modeled P-T path for active subduction zones (model D80; Syracuse et al., 2010), the patterns of carbonate solubility (C in ppm in aqueous fluids in equilibrium with $CaCO_3$, Kelemen and Manning, 2015), and the breakdown boundaries of lawsonite in the Ca-Al-Si-O-H and MORB + H_2O systems. The peak P-T estimates for the Corsica eclogites (star) are from Vitale Brovarone et al. (2011a). Note that the Corsica peak P-T conditions correspond to an important zone of dehydration in the MORB system at the blueschist-eclogite transition zone, which mainly relate to the breakdown of lawsonite in this system.

two main geological systems on the island are Hercynian Corsica and Alpine Corsica. Hercynian Corsica represents the largest part of the island and was only weakly affected by the Alpine orogeny, with the exception of the most external units of the Corsican paleo-margin (External Continental Units, Fig. 2A) that underwent blueschist-facies metamorphism during Alpine subduction. Alpine Corsica occupies the northeastern part of the island and mainly consists of Tethyan metaophiolites and metasediments of the Schistes Lustrés complex, equivalent to the Ligurian-Piemonte units of the Western Alps (Caron and Delcey, 1979; Lagabrielle and Lemoine, 1997; Vitale Brovarone et al., 2013). Weakly metamorphosed equivalents of these units are also exposed in the Nappes Supérieures (Rossi et al., 2002; Marroni and Pandolfi, 2003), and represent a good proxy for Tethyan ophiolites prior to Alpine metamorphism. The Schistes Lustrés complex comprises several units that preserve their primary Tethyan tectonostratigraphic coherence (mantle ultramafics ± metagabbros followed upsection by metavolcanics and metasedimentary cover rocks) but differ in their structural, lithological and metamorphic features (Lagabrielle and Lemoine, 1997; Vitale Brovarone et al., 2011a; Meresse et al., 2012; Vitale Brovarone et al., 2013, 2014) (Fig. 2). This study focuses on the Lawsonite-eclogite-facies unit. This unit consists of a well-preserved section of a Tethyan ocean-continent transition lithosphere (OCT in Fig. 2) characterized by lithological suites similar to slow-spreading oceanic crust, such as serpentinites, metabasalts, and metagabbros (Jurassic), together with the characteristic presence of slivers of continental basement rocks interpreted as continental extensional allochthons (Vitale Brovarone et al., 2011a; Meresse et al., 2012; Beltrando et al., 2014). These rocks are capped by their primary Mesozoic metasedimentary cover rocks.

2.1. Metamorphic evolution of lawsonite eclogites in Alpine Corsica

The Alpine metamorphism in the Schistes Lustrés ranges from low-grade blueschist-facies (ca. 350 °C, 1.5 GPa) to lawsonite eclogite-facies conditions (ca. 530 °C, 2.3 GPa) (Fig. 1). A recent review of the available P-T estimates including a belt-scale thermometric dataset can be found in Vitale Brovarone et al. (2013) (see also Vitale Brovarone et al., 2014 for updates), and only the main metamorphic features of the lawsonite eclogite-facies terranes are reported in the following. Lawsonite eclogite-facies rocks in Alpine Corsica are well

Please cite this article as: Brovarone, A.V., et al., Intra-slab COH fluid fluxes evidenced by fluid-mediated decarbonation of lawsonite eclogite-facies altered oceanic metabasalts, Lithos (2018), https://doi.org/10.1016/j.lithos.2018.01.028

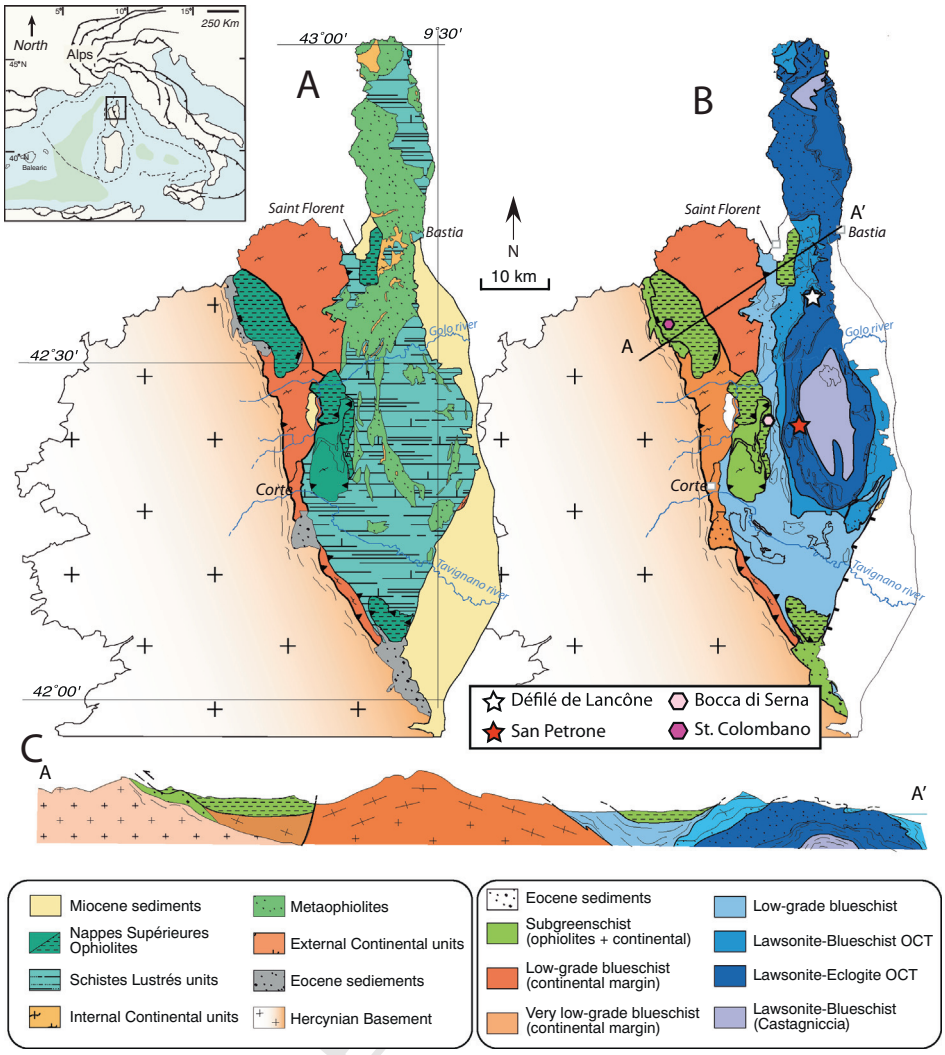

Fig. 2. (A) Simplified geological map of Alpine Corsica. (B) Metamorphic map of Alpine Corsica. The stars in (B) refer to the two selected, eclogite-facies case studies, and the two low-grade equivalents.

preserved and include assemblages indicating the transition from garnet blueschist to eclogite sensu stricto (omphacite-garnet-rich) (Caron and Péquignot, 1986; Miller et al., 2000; Healy et al., 2009; Ravna et al., 2010; Vitale Brovarone et al., 2011b; Vitale Brovarone et al., 2014). A large thermometric dataset based on Raman spectroscopy on the carbonaceous material (RSCM) in this unit points to the peak T ranging from ~460 °C in the northern part to ~540 °C in the southern part of the unit across the belt (Vitale Brovarone et al., 2013). Abundant lawsonite and glaucophane inclusions in the eclogitic garnet indicate prograde metamorphism at HP/LT conditions in the lawsonite-blueschist facies. The peak, lawsonite-eclogite-facies assemblages in the metabasaltic suites are strongly controlled by the whole-rock composition, with two main end-members being omphacite(s) + lawsonite + garnet + titanite + phengite (eclogite-type) and amphibole(s) + lawsonite + garnet + titanite + phengite (blueschist-type) (Miller et al., 2000; Ravna et al., 2010; Vitale Brovarone et al., 2011b). Local P-T estimates are available mainly from pseudosection modeling of mafic rocks. In the Défilé de Lancône, pseudosections for meta-pillow basalts yield T of about 450–500 °C and P in the range 1.9–2.6 GPa (Ravna et al., 2010). In the Monte San Petrone, prograde (450 °C, 1.8 GPa; 480 °C 2 GPa) and peak (520 ± 20 °C; 2.3 ± 0.1 GPa) T conditions are slightly higher than the Défilé de Lancône (Vitale Brovarone et al., 2011b), consistent with the regional RSCM dataset.

Overall, the reconstructed prograde P-T evolution matches the range of P-T paths for most active subduction zones by Syracuse et al. (2010) (Fig. 1). The retrograde path of the Corsican eclogites is poorly constrained, but the preservation of lawsonite suggests relatively cold and/or static conditions.

The peak Alpine HP-LT metamorphism of the lawsonite-eclogite terranes was dated at ca. 34 Ma by means of U-Pb zircon, Lu-Hf garnet and Ar-Ar phengite geochronology (Brunet et al., 2000; Martin et al., 2011; Vitale Brovarone and Herwartz, 2013). Other estimates include a Sm/Nd age of ~83 Ma (Lahondère and Guerrot, 1997) and a scattered Ar-Ar dataset ranging from 40 to 65 Ma (Brunet et al., 2000), but these estimates are likely not relevant for the metamorphism studied herein (see discussion in Vitale Brovarone & Herwartz, 2013).

3. Observations from very low-grade carbonated basalts

In order to improve our understanding of the metamorphic evolution of carbonated metabasalts at HP conditions, we made observations in weakly metamorphosed ophiolitic units from Alpine Corsica, the Nappes Supérieures (Fig. 2). A detailed description of these low-grade materials is beyond the scope of this study, and only the most representative features are reported here for the purpose of providing a general view of the (sub)seafloor hydrothermal alteration of the Corsican rocks prior to subduction. We selected metabasalts from both the San Colombano pass (Balagne Nappe) (Marroni and Pandolfi, 2003) and the Bocca di Serna pass (Vitale Brovarone et al., 2014). In both cases, pillow basalts are well exposed and capped by radiolarian metacherts.

Please cite this article as: Brovarone, A.V., et al., Intra-slab COH fluid fluxes evidenced by fluid-mediated decarbonation of lawsonite eclogite-facies altered oceanic metabasalts, Lithos (2018), https://doi.org/10.1016/j.lithos.2018.01.028

The Alpine metamorphic conditions did not exceed ca. 300 °C and 0.4 GPa (Vitale Brovarone et al., 2013). Metabasalts from both areas exhibit widespread evidence of seafloor hydrothermal alteration and carbonate precipitation, even though important mineralogical variations are observed between the two localities.

In the San Colombano metabasalts (e.g. sample 2cor14-2), carbonate is found as filling material in hollow pillows, resulting in characteristic "heater-like" structures (alternating basalt ceilings and hollows filled by carbonate) that are interpreted to form during progressive cooling of pillow basalts and then filled by hydrothermal products (Fig. 3A; cf. Ballard and Moore, 1977). These veins contain mostly calcite, together with chlorite and minor quartz, sulfides, and fine-grained hematite.

In the Bocca di Serna basalts, a complex network of veins is found in the lowermost portion of the exposed basalt section (Fig. 3B,C). The veins (e.g. sample Cor16-62a) mainly consist of quartz, Ca carbonate, epidote and albite. Epidote + quartz-bearing veins are late with respect to albite-bearing veins, whereas carbonate is present in both vein generations. Both albite and epidote are present preferentially at the vein selvages. In some portions of the basalt section (e.g. sample Cor16-62b), these phases are more pervasively distributed and contain tiny hematite crystals conferring a reddish color to the rock (Fig. 3D). These domains possibly reflect the hydrothermal replacement of the host basalt by newly formed silicates and carbonate. Evidence for massive sulfide deposits in these low-grade units was not found; however, sulfide deposits were exploited in gabbros close by the Bocca di Serna pass (J.P. Santori, personal communication).

Fig. 4 shows two examples of inherited seafloor hydrothermal veins from the low-grade terranes in comparison with some lawsonite eclogite-facies analogues that will be described in detail in the following.

4. Lawsonite eclogite-facies metabasalts and distribution of carbonated eclogites

Metabasalts are widespread in the lawsonite-eclogite-facies unit and form large bodies locally extending for several tens of km. The samples selected for this study are from two localities: the Défilé de Lancône and Monte San Petrone areas (Fig. 2, and S1 for structural relationships) (Miller et al., 2000; Ravna et al., 2010; Vitale Brovarone et al., 2011a, 2011b). In the Défilé de Lancône, metabasalts form a thick sequence (200 m) including various types of well-preserved pillow shapes (bulbous, flattened, elongate and hollow pillow), pillow metabreccias and hyaloclastites. The metabasaltic sequence lies on a large body of serpentinized peridotites capped by a rather thin layer of highly sheared metagabbros (Fig. S1). Altogether, these rocks form a largely complete Tethyan crustal sequence now overturned in the Alpine stack. Discontinuous lenses of metachert are observed and plausibly represent the original sedimentary cover of the basement sequence, i.e. radiolarian metachert. In the San Petrone area, a large, ~200 m thick body of metabasalts rests above serpentinized peridotites containing rare pods of metagabbro. The limited deformation along this contact, as well as the lithostratigraphic consistency at the regional scale, has been interpreted as the evidence for the preservation of a primary slow-spreading crustal sequence where the volcanic suite directly rests on top of exposed mantle rocks (Vitale Brovarone et al., 2011a; Beltrando et al., 2014).

4.1. Four groups of carbonated eclogites

Corsican carbonated metabasalts can be subdivided into four groups based on the origin and distribution of the carbonate (Fig. 5): (1) seafloor hydrothermal veins preserved in undeformed metabasalts (Fig. 5A–B); (2) carbonated metabasalt sensu stricto (Fig. 5C, see below for definition); (3) metamorphic veins and crack-seals crosscutting metabasalts (Fig. 5D); and (4) deformed carbonate-bearing metabasalts (undifferentiated; Fig. 5E). Late, greenschist-facies carbonate veins are not considered in this compilation (Miller et al., 2001; Miller and Cartwright, 2006). Groups (1) and (2) have lower-grade equivalents in weakly metamorphosed units and represent remnants of seafloor hydrothermal processes, whereas group (3) represents the result of metamorphic processes at HP conditions. Most carbonated metabasalts have a remarkably high amount of garnet compared with the carbonate-free metabasaltic rocks in the study areas (20 vol% vs. <10 vol% in carbonate-free metabasalts). In the Défile de Lancône, carbonate-bearing metabasalts are more abundant in the uppermost part of the volcanic sequence (lowermost structural position in the overturned sequence; Fig. S1A). In the San Petrone area (Fig. S1B), carbonate-bearing metabasalts are more scattered, and no obvious correlation between their distribution and the primary volcanic section can be established.

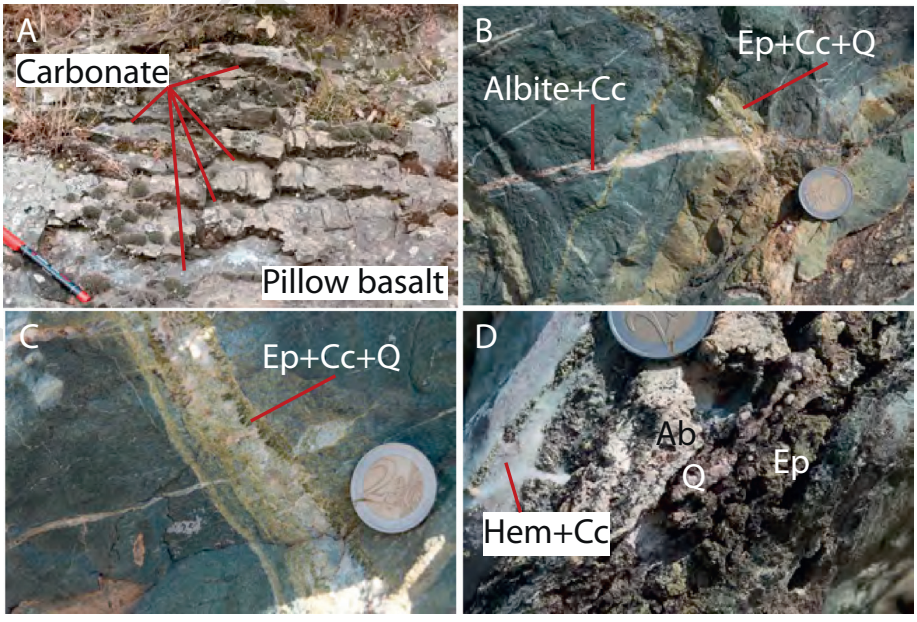

Fig. 3. Examples of hydrothermal alteration in weakly metamorphosed basalts. (A) Heater-like carbonate filling hollow pillows from the San Colombano area. (B–C) Epidote + carbonate + quartz + albite veins in the basalts from Bocca di Serna. (D) Pervasive carbonate + epidote + quartz + albite alteration of basalts from Bocca di Serna.

Please cite this article as: Brovarone, A.V., et al., Intra-slab COH fluid fluxes evidenced by fluid-mediated decarbonation of lawsonite eclogite-facies altered oceanic metabasalts, Lithos (2018), https://doi.org/10.1016/j.lithos.2018.01.028

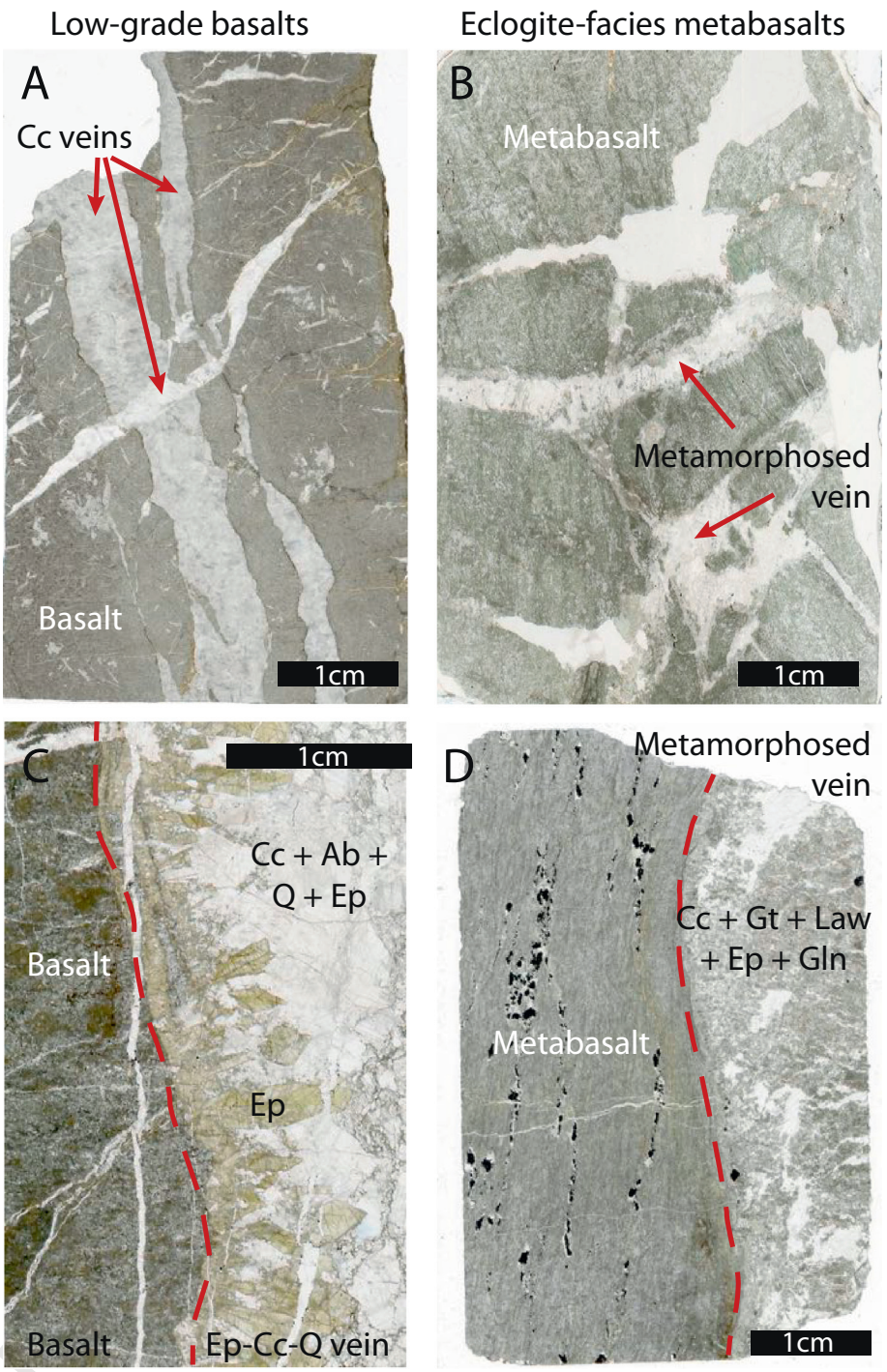

Fig. 4. Comparison between weakly metamorphosed (A, C) and eclogite-facies carbonate-bearing structures. (A) Carbonate-rich veins crosscutting the San Colombano basalts and (B) their equivalents in the San Petrone eclogites (sample OF3156). Note in (A) the presence of multiple vein generations. (C) Epidote + carbonate + quartz + albite veins in the Bocca di Serna basalts and (D) their metamorphosed equivalents in the Défilé de Lancône eclogites (sample Lancône-pillow). See text for detailed description and interpretations.

4.1.1. Group 1: metamorphosed seafloor hydrothermal veins

Different types of seafloor hydrothermal veins are distinguished (Figs. 4A, B, 6A–E). Some pillow metabasalts preserve the 'heater-like' structures characteristic of hollow pillows. These structures typically consist of cm-thick carbonate-rich parallel veins preserved in the pillow's core and extending outward to a more complex network of thinner, randomly oriented veins (Fig. 6B,C; see also Fig. 3A for low-grade precursor). In other cases, carbonate is only found as randomly-oriented veins filling igneous cooling fractures in undeformed metabasalt (Figs. 4B, 5B, 6E). The carbonate in these structures may have two possible origins: hydrothermal carbonate precipitating from seawater circulation, or sedimentary carbonate filling open fractures. A hydrothermal origin is preferred for most of our samples based on the collected dataset (see sample description). Owing to surface carbonate dissolution, these rocks are rarely preserved on the weathered surface (Fig. 6E). Despite that, fresh samples were found both along the Défilé de Lancône in the interior of large pillow basalts, and at San Petrone.

Please cite this article as: Brovarone, A.V., et al., Intra-slab COH fluid fluxes evidenced by fluid-mediated decarbonation of lawsonite eclogite-facies altered oceanic metabasalts, Lithos (2018), https://doi.org/10.1016/j.lithos.2018.01.028

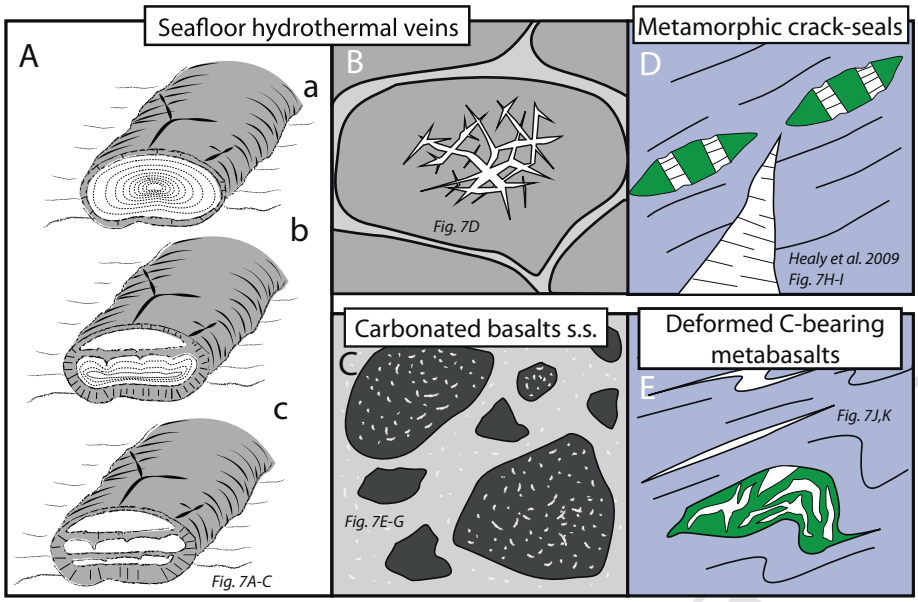

Fig. 5. Cartoons summarizing the different types of carbonated metabasalts observed in Alpine Corsica. (A–C) represent inherited seafloor structures, whereas (D–E) are for either purely metamorphic (D) or undifferentiated (E) structures. (A) Mechanism of hollow pillow formation illustrating the origin of the 'heater-like' structures observed in the field; redrawn after Ballard and Moore (1977). In (a–c), the cavities are then filled by hydrothermal products such as carbonates (see also Fig. 6B,C). In (B), the carbonate veins are confined to the inner part of the pillow (see Figs. 4B, 6E). (C) Carbonated metabasalt s.s. This type of carbonate-bearing metabasalt is most commonly observed in basaltic metabreccias (see Fig. 6F for field examples). The carbonate distribution is pervasive and results from replacement of primary magmatic minerals, e.g., olivine. (D) Carbonate-bearing metamorphic crack-seals. The cartoon shows two types of metamorphic crack seals; filling material in boudinaged eclogite pods hosted in foliated blueschists, and discordant carbonate-bearing veins crosscutting the HP schistosity. (E) Cartoon illustrating different types of deformed carbonate-bearing metabasalts for which a clear origin (seafloor vs. subduction) is not obvious.

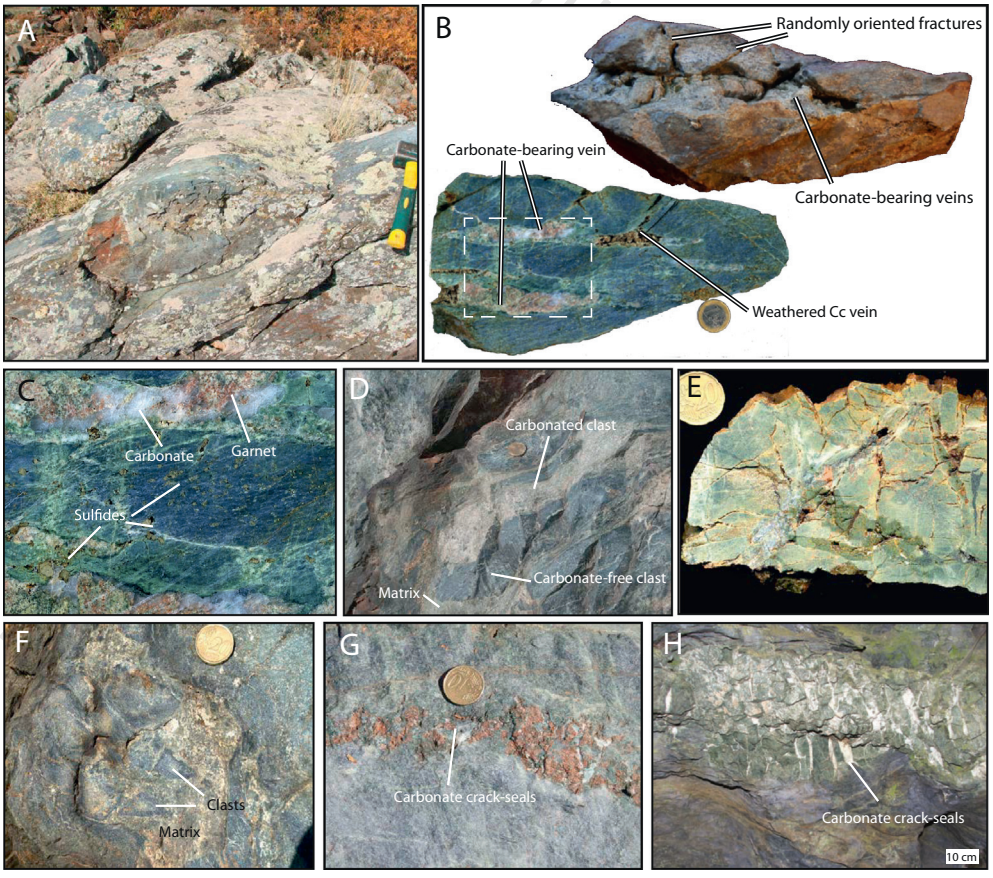

Fig. 6. Examples of Corsican carbonate-bearing metabasalts. Group 1: (A) Examples of preserved pillows metabasalts from the San Petrone area. Carbonates are present in the fractures in pillow's core. (B–D) Hollow pillow metabasalts from the Lancône valley. Note the main (horizontal) fractures extending laterally to a more complex network of fractures. In (C), note the abundance of garnet (reddish zones) within the carbonate-rich domains. (E) Example of weathered, randomly oriented, carbonate-bearing veins in the San Petrone metabasalts. The carbonate filled the open fractures. Group 2: (F) Carbonated metabasalts (sensu stricto) forming both clasts and matrix in pillow metabreccias. Group 3: (G–H) Carbonate + omphacite ± garnet ± phengite metamorphic crack-seals in the metabasalts from the San Petrone area. (For interpretation of the references to color in this figure legend, the reader is referred to the web version of this article.)

Please cite this article as: Brovarone, A.V., et al., Intra-slab COH fluid fluxes evidenced by fluid-mediated decarbonation of lawsonite eclogite-facies altered oceanic metabasalts, Lithos (2018), https://doi.org/10.1016/j.lithos.2018.01.028

4.1.2. Group 2: carbonated metabasalts sensu stricto

Carbonated metabasalts sensu stricto are herein distinguished from the other carbonate-bearing metabasalts. In these rocks, the carbonate is diffusely distributed in the matrix of undeformed metabasalts and is most probably the result of seafloor hydrothermal replacement of primary olivine or filling of disseminated vesicles (Alt and Teagle, 1999), rather than crack-filling precipitation processes. These rocks are most typically found as metabasaltic clasts or matrix material in hyaloclastites or pillow metabreccias (Fig. 6F). Carbonated metabasalts sensu stricto are common along the easternmost part of the Défilé de Lancône metabasaltic suite.

4.1.3. Group 3: carbonate-bearing metamorphic crack-seals

Carbonate-bearing metamorphic veins are locally abundant within the metabasaltic suite of the San Petrone area, whereas they are rarer in the Défilé de Lancône suite. Most of them were stretched and made subparallel to the main regional foliation, but some still show clear crosscutting relationships with the deformed metabasalt hosts (Healy et al., 2009; Ravna et al., 2010; Vitale Brovarone et al., 2011b). The typical assemblage consists of rod-shaped carbonate and omphacite, together with coarse-grained phengite; apatite and rare garnet can be easily identified in hand specimen.

4.1.4. Group 4: deformed carbonate-bearing metabasalts

Owing to local intense deformation, the genesis of these rocks cannot be easily ascribed to one of the above groups. One type—quite common in the Défilé de Lancône area—exhibits a well-developed schistosity of alternating blue with light-blue/green layers. The variable thickness of the layers ranges from a few millimeters to several centimeters. Carbonate in these rocks may also have a sedimentary rather than hydrothermal origin.

5. Sample description and mineral chemistry

In this section, we present the mineral assemblages, microstructures and mineral chemistry for the two key carbonated metabasalt types central to this study, i.e. metamorphosed seafloor hydrothermal veins (Group 1; three samples) and metamorphic crack-seals (Group 3; one sample). Ar-Ar data are also presented for phengite in Group 3 metamorphic veins. A description of carbonated metabasalts sensu stricto (Group 2) and deformed carbonated metabasalts (Group 4) is beyond the aim of this work. Analytical methods are described in the Supplementary Material.

5.1. Group 1: Metamorphosed seafloor hydrothermal veins

Different types of primary hydrothermal veins are recognized, and show contrasting metamorphic transformations. The two most representative ones are described as follows.

5.1.1. Large carbonate veins in pillow metabasalts

5.1.1.1. Sample Lancône-pillow. This sample was used for in-situ garnet O isotope analyses (see Section 6). It can be subdivided into two parts: the carbonate-free metabasalt host and a carbonate-rich hydrothermal vein (Fig. 6B,C). The host metabasalt mainly consists of glaucophane, lawsonite, actinolite, garnet, titanite, and sulfides, with garnet amount <5 vol%. These phases form a fine-grained, weakly deformed matrix that commonly preserves the original basaltic aphyric texture.

The carbonate-rich hydrothermal vein consists primarily of carbonate, garnet, and lawsonite, together with epidote, green-amphibole, chlorite, blue-amphibole, and sulfides (Fig. 7A).

Calcite is the dominant *Ca carbonate* polymorph in the rock. Nevertheless, Raman spectroscopy revealed the preservation of aragonite included in garnet, lawsonite, and pyrite (Fig. S2), as also observed in the other selected samples (see also sample Lancône12-6). *Garnet* in the carbonate veins is more abundant than in the host metabasalt (Fig. 7B), is present as isolated or aggregated crystals, contains inclusions of Ca carbonate, lawsonite, quartz, and epidote, and is partially replaced by late chlorite (Fig. 7C). The garnet compositional zoning is complex, and two main populations can be distinguished based on X-ray compositional mapping. The first one (Gt1; Fig. 7D) has an Mn-richer core [XSps = 0.2; XGrs = 0.4; XAlm = 0.4] and Mn-poorer rim [XSps = 0.0; XGrs = 0.7; XAlm = 0.3]. The second garnet generation (Gt2; Fig. 7E,F) is Mn-poor and displays a patchy compositional zonation with alternating Ca-richer [XGrs = 0.6; XAlm = 0.4; XSps = 0] and Ca-poorer [XGrs = 0.4; XAlm = 0.6; XSps = 0] compositions. In both garnet generations, a late Mn-rich shell is commonly observed. *Epidote* is widespread as both prograde inclusions in Gt2 (Ep1) and as a secondary phase after lawsonite (Ep2). Ep1 might also be preserved in the matrix. *Lawsonite* is found as inclusions in garnet and sulfides (Fig. 7F), and as large idioblastic crystals in the matrix (Fig. 7A). Both lawsonite types formed at the expense of Ep1. *Green-amphibole* forms idiomorphic crystals and is present in higher modal proportion along the contact with the host metabasalt. *Blue-amphibole* forms isolated crystals dispersed in the calcite matrix, and is generally well preserved. *Chlorite* is common in the rock and is found as a prograde-to-peak phase and retrograde product after garnet or amphibole (Fig. 7C). *Sulfides* are extremely abundant in both the vein and the host metabasalt compared to the average metabasaltic rocks of Corsica; they are found as tiny crystals dispersed in the calcite matrix or as inclusions in garnet, lawsonite, and epidote. In the host metabasalt, sulfides are locally arrayed, suggesting precipitation along seafloor and/or metamorphic veins (Fig. 4D). Late *albite* is found as a retrograde product along cracks, grain boundaries and in pressure shadows around sulfides (Fig. 4D).

5.1.1.2. Sample Lancône12-6. This sample was used for thermodynamic calculations (see Sections 7 and 8). It was collected along the Défilé de Lancône, and belongs to a deformed large hydrothermal vein equivalent of sample Lancône-pillow (Fig. 6D). It has a homogeneous, fine-grained isotropic texture characterized by a light-colored matrix including small reddish garnet and variably oxidized sulfides. The main mineral phases are, in order of decreasing modal abundance, lawsonite, albite, garnet, calcite, epidote, amphiboles, chlorite, omphacite, quartz, titanite, pyrite, and apatite.

Lawsonite is well preserved and shows very little retrograde overprint (Fig. 8). It is common both in the rock's matrix and as inclusions in other phases, most notably garnet and pyrite (Fig. 8). In the matrix, lawsonite has a typical tabular idioblastic habit, and includes mostly quartz with lesser carbonate. Lawsonite included in garnet may have different habits: it is idiomorphic when in close association with epidote (Fig. 8D,E), whereas it is xenomorphic and rounded in association with carbonate and quartz when included in garnet (Fig. 8F,G).

Carbonate is present as xenomorphic crystals, aggregates in the matrix, or as inclusions in other phases such as garnet (Fig. 8E–G), lawsonite (Fig. 8H), and pyrite. Like the previous samples, this rock contains Ca carbonate only, which is found as both matrix calcite and fresh aragonite inclusions (Fig. 8H).

Epidote is found in two main microstructural positions, (1) as inclusions in garnet (Ep1) [$Fe^{3+}/(Fe^{3+}+Al) = 0.16$] (Fig. 8B); (2) as texturally late pseudomorphic products after garnet (Ep2a) [$Fe^{3}/(Fe^{3}+Al) = 0.18$], matrix lawsonite (Ep2b) [$Fe^{3}/(Fe^{3}+Al) = 0.07$] (Fig. 8C) and, together with albite and chlorite, amphibole (Ep2c). Ep1 displays a complex zonation observed in backscatter (Fig. 8D,E).

Garnet forms poikiloblastic, idiomorphic to sub-idiomorphic crystals and aggregates. Single crystals range in size from about 100 to 500 μm. Two end-member types of garnet can be distinguished. The first one (Gt1) includes clusters of lawsonite, aragonite, quartz and epidote (Fig. 8A,F,G). Gt1 is compositionally zoned, with zonation ranging from normal or inverse Mn bell-shaped zonation. The second one (Gt2) includes large Ep1 crystals and is chemically homogeneous [XGrs = 0.4; XAlm = 0. 57; XSps = 0.02; XPy = 0.01] (Fig. 8B,I). The

Please cite this article as: Brovarone, A.V., et al., Intra-slab COH fluid fluxes evidenced by fluid-mediated decarbonation of lawsonite eclogite-facies altered oceanic metabasalts, Lithos (2018), https://doi.org/10.1016/j.lithos.2018.01.028

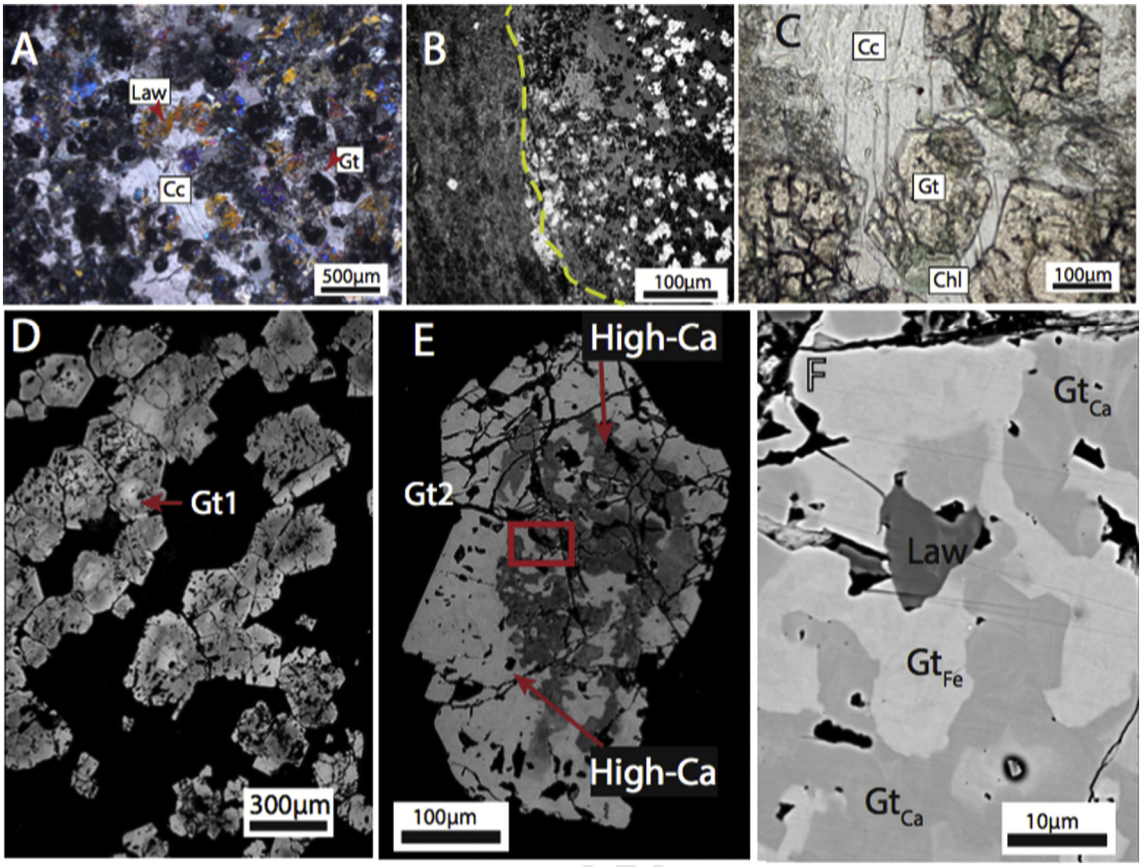

Fig. 7. Photomicrographs of sample Lancône-pillow (Group 1: inherited hydrothermal vein). (A) Representative microstructure of the carbonate-rich hydrothermal vein showing abundant garnet and lawsonite in a calcite matrix. Cross-polarized light (XPL). (B) Backscatter electron (BSE) image of the interface between the metamorphosed carbonate channel (right) and the host metabasalt (left) in sample Lancône-pillow. Note the much greater abundance of garnet in the vein relative to the host metabasalt. (C) Late chlorite overprinting garnet. Plane-polarized light (PPL). (D) BSE image of zoned Gt1 in the inherited hydrothermal vein. The bright cores are Mn-richer, while the bright rims are Fe-richer. (E) BSE image of Gt2 alternating patches of Ca-richer and Ca-poorer compositions. (F) Detail of (E) (red box in E for location) showing the complex chemical zoning of Gt2. Note also a lawsonite inclusion. (For interpretation of the references to color in this figure legend, the reader is referred to the web version of this article.)

relative modal amounts of the different garnet types vary from one to another thin section. Garnet showing intermediate features between Gt1 and Gt2 are also observed. Both garnet types locally include sulfides. Zoned crystals of *amphibole* with glaucophane cores and actinolite rims are widespread. Isolated actinolite crystals are also found, and may be either a peak or a retrograde phase. *Chlorite* aggregates are deep green and pseudomorphically replace garnet and amphibole. Chlorite has Mg# of 0.56–0.58 ($Mg/[Mg + Fe^{2+}]$). *Pyrite* forms sub-idiomorphic crystals or aggregates, and includes lawsonite, carbonate, and quartz. *Quartz* is common as inclusions in lawsonite, garnet, and pyrite (Fig. 8C,E,F–G). In the matrix, quartz is scarce in the presence of Gt1, but is more abundant in the vicinity of Gt2 (Fig. 8I). *Albite* is widespread in this sample, and is present as large poikiloblastic crystals in the matrix, as filling material in fractured garnet, or along grain boundaries (Fig. 8I,G). In some cases, albite is found as inclusions in garnet (Fig. 8G). However, the albite inclusions are systematically connected by late cracks and are interpreted as a retrograde replacement of former inclusions. Tiny *apatite* crystals are disseminated in the rock's matrix.

5.1.2. Small carbonate veins in pillow metabasalts (sample OF3156)

Sample OF3156 belongs to the core of a well-preserved pillow metabasalt. The metabasalt preserves primary igneous textures that have been completely overgrown statically by a very fine-grained mineral assemblage typical of the lawsonite-eclogite facies (omphacite + lawsonite + garnet) (Fig. 9A). Garnet in the host metabasalt is rare and is crowded with tiny titanite inclusions. The carbonate-bearing veins dominantly consist of calcite, together with lawsonite, omphacite, and garnet (Fig. 9B–C). All vein minerals display a larger grain size compared to the host metabasalt. In thin section, calcite exhibits concentric square/pseudo-hexagonal shapes that plausibly represent preserved aragonite basal sections now converted to calcite (Fig. 9B). Lawsonite-rich selvages commonly formed at the contact between the carbonate-bearing veins and the metabasalt wall (Fig. 9C), and may have developed via either transformation of primary Ca-rich hydrothermal products (e.g. epidote), or by the interaction between the carbonate vein and the host metabasalt (decarbonation reactions) during subduction. Omphacite in the vein is zoned, with aegirine-richer cores and omphacite-richer rims (Fig. 9C). The random vein orientation relative to the Alpine regional structures is consistent with the hypothesis of oceanic hydrothermal fracturing, but the reworking of these fractures during HP fluid circulation cannot be excluded.

5.2. Group 3: carbonate-bearing metamorphic crack-seals

The selected sample (*OF3322*) is characterized by two superimposed veining events. The first vein generation is composed of massive garnets and coarse-grained omphacite aggregates, whereas the second is dominated by Ca carbonate, phengite, and minor omphacite (Fig. 10). A detailed description of the first vein generation is beyond the aim of this study and has been already given in previous works (Healy et al., 2009; Vitale Brovarone et al., 2011b). The chronological relationships between the two veining events are clearly depicted by intense hydrofracturing of garnet and omphacite and sealing by Ca carbonate and phengite (Fig. 10C,D). A second generation of omphacite forms

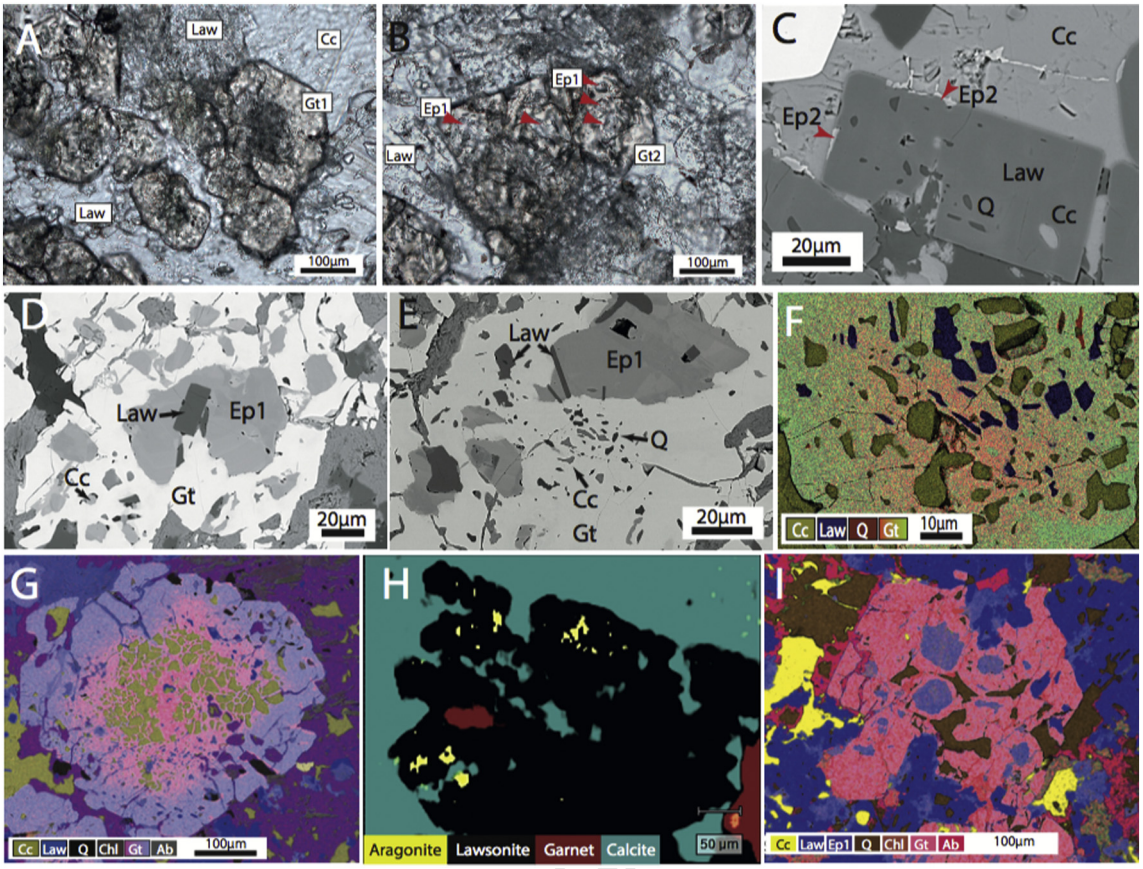

Fig. 8. Representative microstructures of sample Lancône12-6 (Group 2: carbonated metabasalt sensu stricto). (A) Example of Gt1. Note the clouded core containing abundant rounded carbonate inclusions (see also panel G). (B) Example of Gt2. See also Figure I. (C) BSE image showing an idiomorphic lawsonite crystal including quartz and carbonate. In some crystals, the carbonate included in lawsonite is still fresh aragonite (Fig. S2). Note also the development of Ep2 along the edge of the lawsonite crystal. (D–G) Examples of inclusions in Gt1. In (D) note the presence of an idioblastic lawsonite crystal growing on Ep1, both included in Gt1. This texture suggests a prograde partial conversion of epidote into lawsonite prior or during the garnet growth. (F–G) Composite X-Ray compositional maps showing the characteristic textures of Gt1 in sample Lancône12-6. In (G), note the abundant carbonate inclusions in Gt1 core. The garnet zoning is mainly due to variations in Mn, which is richer in the core and poorer in the rim. In both maps, note the included assemblage consisting of xenomorphic carbonate, quartz and lawsonite suggesting the garnet-forming reaction (1). (H) Raman map showing the preservation of fresh aragonite as inclusions in both lawsonite and garnet, and a complete conversion into calcite in the matrix. (I) Compositional map of Gt2 in sample Lancône12-6. Note the lack of significant zoning in this garnet type, the presence of atoll-like inclusions of Ep1, and the presence of matrix quartz in association with Gt2. Note also the presence of late albite. Abbreviations: Law: lawsonite; Q: quartz; Ab: albite; Cc: Ca carbonate; Gt: garnet; Chl: chlorite; Ep: epidote.

small, idioblastic crystals dispersed in the carbonate matrix. Phengite has a high Si content (Si = 3.5–3.6 atoms per formula unit, based on 11 oxygens, Table 2). The association of high-Si phengite, newly formed omphacite and the overall freshness of the early garnet and omphacite assemblage altogether support the hypothesis of carbonate precipitation at HP conditions. Rarely, the phengite crystals are replaced by late albite, indicating at least some degree of retrogression.

We performed Ar-Ar geochronology on phengite from these veins. Single crystals of highly substituted phengite (Si = 3.5–3.6 a.p.f.u.) were separated from two different samples (M9-53a and M9-53b, equivalent to samples 2cor12-8, 2cor12-11 and *OF3322*) and analyzed by the step-heating method. The results are shown in Fig. 11 and Supplementary Table 1. The first sample is characterized by an initial slight stepping-up spectrum from 26.8 ± 1.3 Ma to 28.5 ± 0.2 Ma, followed by a well-defined plateau at 29.2 ± 0.6 Ma. The second sample yields age spectra characterized by a plateau age at 25 Ma (25.3 ± 0.5 and 25.0 ± 0.7 Ma on two separate crystals).

6. Whole-rock and in-situ C and O stable isotopes

We performed whole-rock carbonate $\delta^{13}C$ and $\delta^{18}O$ analyses on four samples from the Défilé de Lancône and San Petrone areas (Table 1), as well as in-situ $\delta^{18}O$ garnet isotope analysis by SIMS in order to investigate the possible contribution of decarbonation reactions to the isotopic signature of newly-formed Ca-rich garnet.

Tables 3 and S2 and Figs. 12 and 13 show the results in per mil (‰) with respect to the international PDB standard for C and SMOW for oxygen. The hydrothermal veins from the Défilé de Lancône (e.g. sample Lancône-pillow) have $\delta^{13}C_{PDB}$ of −1 to −0.5‰ and $\delta^{18}O_{SMOW}$ of 9‰. The carbonated metabasaltic clast (sample Lancône12-6) has $\delta^{13}C$ of 1‰ and $\delta^{18}O$ of 11.6‰. Finally, the carbonate-bearing eclogitic crack-seals (samples OF3322, 2cor12-8 and 2cor12-11) have $\delta^{13}C$ of 1.2‰ and $\delta^{18}O$ of 11.6‰. The $\delta^{13}C$ values are comparable with the lowermost values obtained by Miller et al. (2001) in Corsican eclogite-facies metabasites (−1 to 3‰) (Fig. 12A). Conversely, the $\delta^{18}O$ values are lower than the samples analyzed by Miller et al. (2001) (13 to 20‰).

For in-situ $\delta^{18}O$ garnet analyses, we selected garnet crystals with alternating Ca-poorer and Ca-richer zones (patchy, Mn-poor Gt2, Fig. 12B) in sample Lancône-pillow. Sixty point-analyses were performed in cut thin sections on six garnet crystals, and yield average $\delta^{18}O$ values of 5.1 ± 0.4‰ (2SD□□n = 41□□) and 4.83 ± 0.4‰ (2SD□□n = 19□□) for the Ca-poorer and Ca-richer garnets, respectively (Fig. 12C). Using bulk Ca carbonate and in-situ garnet $\delta^{18}O$ values for sample Lancône-pillow, and the oxygen fractionation factors by Zheng (1993), a T of ~500 °C was obtained for the carbonate-garnet equilibrium, which is consistent with other temperature estimates in this area.

Please cite this article as: Brovarone, A.V., et al., Intra-slab COH fluid fluxes evidenced by fluid-mediated decarbonation of lawsonite eclogite-facies altered oceanic metabasalts, Lithos (2018), https://doi.org/10.1016/j.lithos.2018.01.028

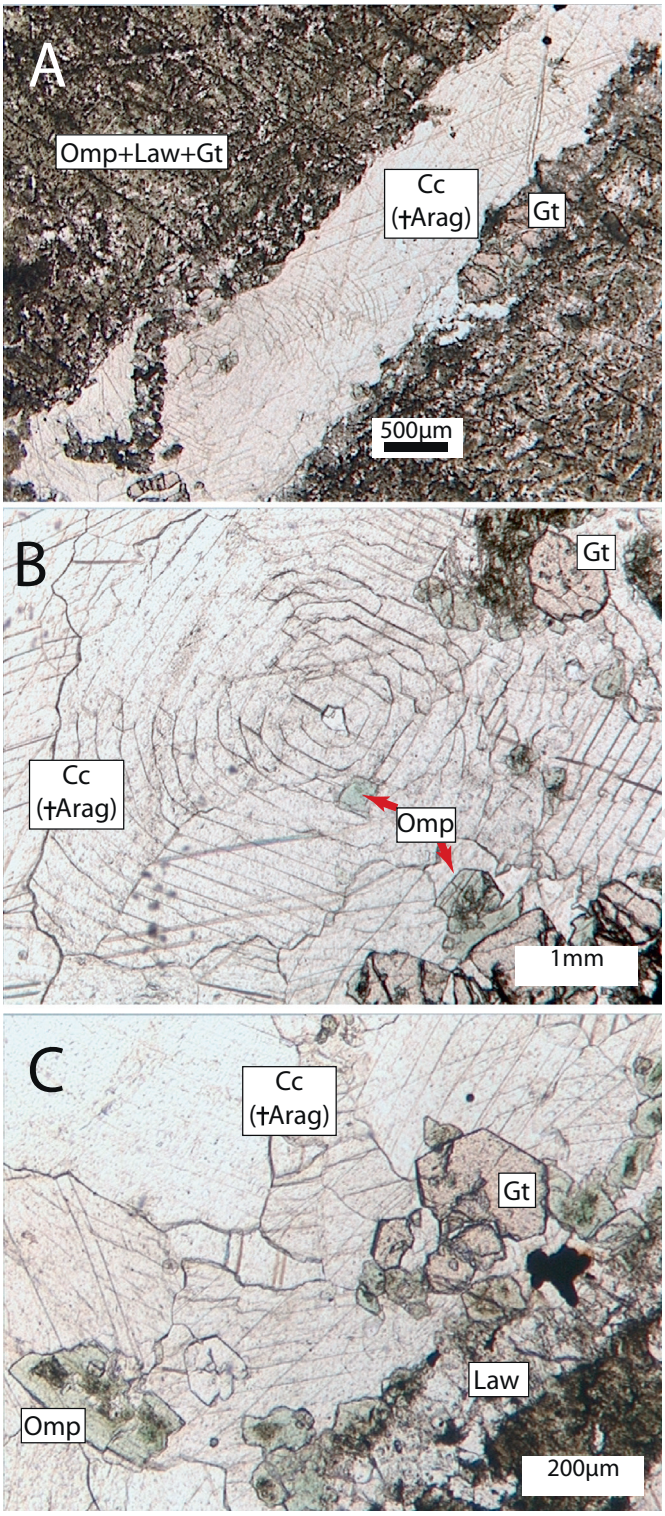

Fig. 9. Photomicrographs of sample OF3156 [inherited, randomly oriented carbonate veins (Group 1) from the San Petrone metabasalts]; PPL. (A) Carbonate vein crosscutting an undeformed, eclogite-facies metabasalt. Note the preservation of the primary igneous texture overgrown by dominant omphacite and lawsonite, and minor garnet. Along the vein, two large (ca. 2 mm) pseudohexagonal concentric structures are observed (cf. B for close up), and probably correspond to former aragonite basal sections now converted to calcite. (C) Example of lawsonite eclogite-facies reequilibration in the inherited vein. Note the presence of garnet, zoned omphacite and lawsonite, the latter being concentrated at the vein wall (bottom-right).

7. Garnet formation and decarbonation reactions

We investigated in more detail the most likely garnet-forming reactions and their contributions to the C budget of the rock. The metamorphic evolution of this sample is summarized in Fig. 13. The large variety of garnet compositions and mineral inclusions in our samples suggest local-equilibrium domains imposed by the precursor textures and mineralogy of the hydrothermally-altered basalt.

Gt1 in Group 1 samples Lancône-pillow and Lancône12-6 contains xenomorphic inclusions of lawsonite, aragonite, quartz ± Ep (Fig. 8E–G). The relict reactants included in the garnets thus suggest the reactions:

$$\text{Lawsonite} + 2\ \text{Aragonite} + \text{Quartz} = \text{Grossular} + 2\ CO_2 + 2\ H_2O \quad (1)$$

$$2\ \text{Clinozoisite} + 5\ \text{Aragonite} + 3\ \text{Quartz} = 3\ \text{Grossular} + 5\ CO_2 + H_2O \quad (2)$$

The common presence of quartz as inclusions in garnet and the textural dependence of Gt1 and Gt2 development on the availability of local quartz are consistent with these prograde reactions. The relative contributions of reactions (1) and (2) in the sample are variable, and depend on the extent of local re-equilibration of the sample (i.e. Ep1 to lawsonite) prior to garnet formation. Gt2 is texturally associated with Ep1 (Fig. 8I), and the chemical homogeneity of Gt2 and Ep1 suggests that the two phases have reached equilibrium by exchanging compositions via Reaction (2) and the redox reaction:

$$3\ \text{Epidote} = \text{Almandine} + 2\ \text{Grossular} + 1.5\ H_2O + 0.75\ O_2 \quad (3)$$

In this reaction, O_2 is included only as a redox indicator, but not considered as a fluid species in mass balance analysis due to its infinitesimal concentration.

The presence of Mn- and Fe-rich garnet zones indicates that at least one additional mafic mineral, likely prograde chlorite, participated in the garnet-forming reactions. Reactions (2) and (3) can be coupled to account for the measured composition of Ep1 included in Gt2:

$$[0.48\ \text{Epidote} + 0.52\ \text{Clinozoisite}] + 1.3\ \text{Aragonite} + 0.78\ \text{Quartz} = 0.16\ \text{Almandine} + 1.1\ \text{Grossular} + 0.5\ H_2O + 1.3\ CO_2 + 0.12\ O_2 \quad (4)$$

The garnet composition resulting from reaction (4) between epidote and carbonate is enriched in grossular component [$X_{Grs} = 0.87$; $X_{Alm} = 0.13$], in contrast to the composition of Gt2 in the sample [$X_{Grs} = 0.4$; $X_{Alm} = 0.6$]. Taking the composition of Gt2 as a proxy, the garnet formation resulted from decomposition of the former minerals clinozoisite/epidote, aragonite, quartz, and additional Fe-Mg-Mn-bearing minerals (e.g., seafloor hydrothermal celadonite and/or Fe-oxyhydroxides; prograde chlorite, amphibole). It is worth noting that the reaction between hydrous silicate and carbonate ((1) and (2)) consumes a significant amount of quartz in the rock. These reactions could not take place in standard silica-undersaturated metabasalts, whereas they are favored in seafloor hydrothermal products containing free quartz as a reactant, as observed in the seafloor hydrothermal products preserved in the Corsica metabasalts (Figs. 3, 4C). Nevertheless, our data suggest that the size and initial mineral assemblage of the inherited hydrothermal veins controlled the extent of fluid channelization and magnitude of decarbonation reactions in the rock. As an example, Ep1-bearing large inherited veins in hollow pillow metabasalts (see Figs. 4C,D, 5A, 6B) show extensive decarbonation reactions, whereas Ep-1-free small, inherited cooling fractures in metapillow cores (see Figs. 4A,B, 5B, 6E) do not.

Please cite this article as: Brovarone, A.V., et al., Intra-slab COH fluid fluxes evidenced by fluid-mediated decarbonation of lawsonite eclogite-facies altered oceanic metabasalts, Lithos (2018), https://doi.org/10.1016/j.lithos.2018.01.028

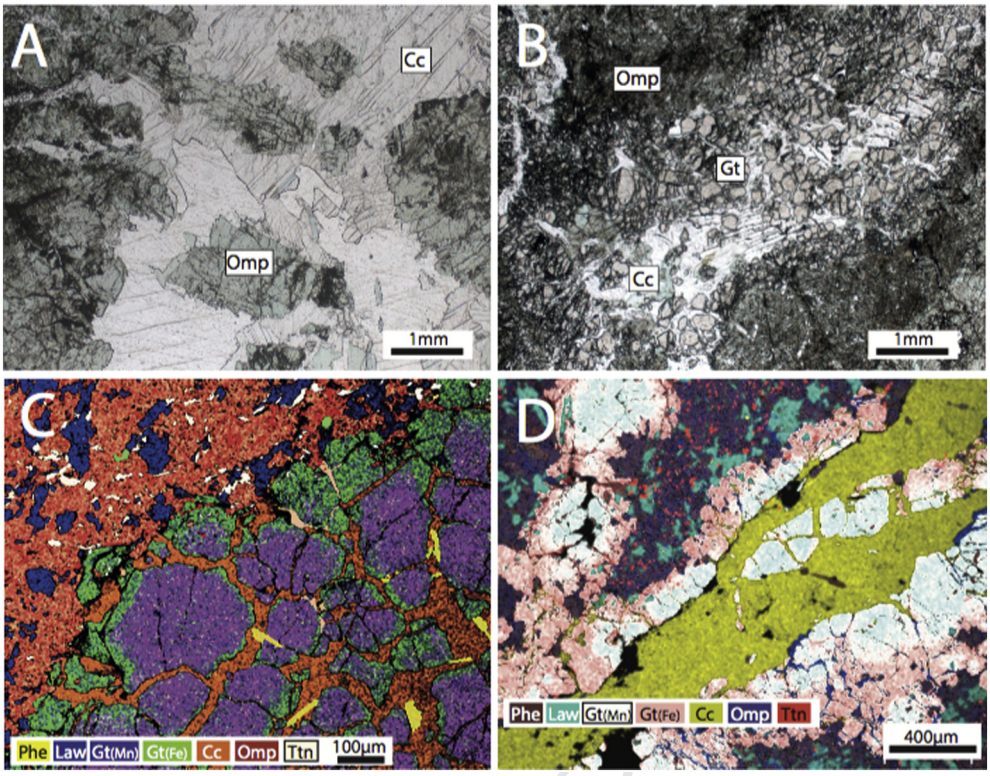

Fig. 10. Photomicrographs (PPL), BSE images and X-Ray composite compositional maps of carbonate-bearing metamorphic crack-seals. The selected example consists of a polyphase vein system including a first omphacite-garnet generation, followed by a second generation consisting of carbonate + phengite ± omphacite. In (A), the first generation assemblage is hydrofractured and sealed by the carbonate-rich assemblage. (B) Detail of a fractured omphacite vein sealed by carbonate. (C–D) Selvage of a composite vein crosscutting the host metabasalt (top-left). The effect of fracturing during carbonate and phengite precipitation is supported by the truncated zonation in the garnet. In (D), note the presence of two garnet veins cutting the host metabasalt (omphacite-lawsonite-titanite zones), only one of which was successively reworked during carbonate precipitation. Abbreviations as Fig. 8, plus Phe: phengite; Omp: omphacite; Ttn: titanite.

8. Fluid composition and time-integrated fluid flux

We conducted phase-equilibrium calculations to link the garnet forming reactions to decarbonation in the lithologic unit. Owing to the compositional and mineralogical microdomains, standard pseudosection modeling based on bulk-rock compositions cannot reflect local phase relations (e.g., Stüwe, 1997; Guevara & Caddick, 2016), especially for the low-temperature (<600 °C) assemblage. We therefore considered single or coupled reactions (1), (2) and (3) to solve local equilibria involving garnet formation in sample Lancone12-6.

We used the internally-consistent thermodynamic dataset of Holland and Powell (1998), a MATLAB-based code package to perform the thermodynamic calculations (Chu and Ague, 2013), and updated activity models (garnet: White et al., 2007; epidote: Holland and Powell, 1998; H_2O-CO_2: Holland and Powell, 2003). The activities of garnet and epidote are calculated using the representative compositions in the prograde assemblage (Lancône12-6: Gt2 $X_{Alm} = 60$; $X_{Grs} = 40$; Ep1: XEp = 16; $X_{Zo} = 84$; Table 2). These calculations were done by considering previous estimates of the prograde P-T path for these rocks (Ravna et al., 2010; Vitale Brovarone et al., 2011b) and the T calculated for the carbonate-garnet isotopic equilibrium. Additional details of thermodynamic calculation are provided in the Supplementary Material. P-T contours are calculated at specified fluid compositions (X_{CO_2}) (reactions (1) and (2)) or oxygen fugacities (f_{O_2}) (reaction (3)) (Fig. 14). For reactions (1) and (2), the assemblage at higher T reaches equilibrium with a higher-X_{CO_2} fluid. The assemblage epidote + garnet

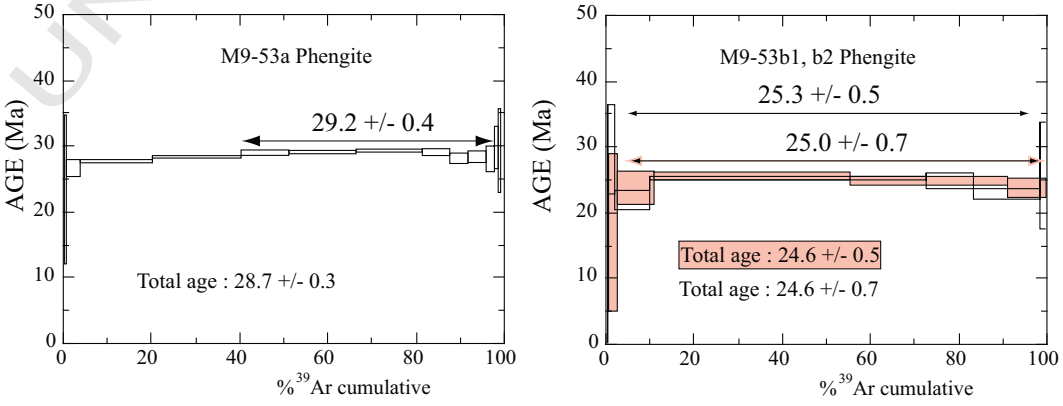

Fig. 11. Ar-Ar phengite plots for two samples of carbonate-bearing crack-seals.

Please cite this article as: Brovarone, A.V., et al., Intra-slab COH fluid fluxes evidenced by fluid-mediated decarbonation of lawsonite eclogite-facies altered oceanic metabasalts, Lithos (2018), https://doi.org/10.1016/j.lithos.2018.01.028

Table 1
Selected samples and analytical strategy.

Sample	Group	Locality	Facies[a]	Peak T[a]	Peak P[a]	Petrography	Mineral chemistry	Thermodynamic modeling	Carbonate bulk $\delta^{13}C$-$\delta^{18}O$	Garnet in-situ $\delta^{18}O$	Phengite Ar-Ar
2cor14-2	1	San Colombano	Sub-greenschist	300 °C	0.4 GPa	X	X				
Cor16-62a	1	Bocca di Serna	Sub-greenschist	300 °C	0.4 GPa	X	X				
Cor16-62b	2	Bocca di Serna	Sub-greenschist	300 °C	0.4 GPa	X	X				
Lancône-pillow	1	Défilé de Lancône	Lawsonite-eclogite	450–500 °C	1.9–2.6 GPa	X	X		X	X	
OF3156	1	San Petrone	Lawsonite-eclogite	500–540 °C	2.2–2.4 GPa	X	X				
Lancône12-6	1	San Petrone	Lawsonite-eclogite	500–540 °C	2.2–2.4 GPa	X	X	X	X		
OF3322	3	San Petrone	Lawsonite-eclogite	500–540 °C	2.2–2.4 GPa	X	X		X		X
2COR12–8/M9-53a[b]	3	San Petrone	Lawsonite-eclogite	500–540 °C	2.2–2.4 GPa	X	X		X		X
2COR12–11/M953b[b]	3	San Petrone	Lawsonite-eclogite	500–540 °C	2.2–2.4 GPa	X	X		X		X
Acor14-16a,c	4	Défilé de Lancône	Lawsonite-eclogite	450–500 °C	1.9–2.6 GPa	X	X				

[a] See text for references.
[b] The two samples are equivalent.

is metastable on the high-pressure side of the lawsonite/epidote transition. At the same P-T conditions, the meta-stable epidote-bearing assemblage is in equilibrium with a fluid of higher X_{CO_2} (dashed curves in Fig. 14) than the lawsonite-bearing assemblage (solid curves in Fig. 14). The f_{O_2} contours of reaction (3) are sensitive to pressure, as discussed by Donohue and Essene (2000) for equivalent redox reactions. The epidote and garnet of interest, if equilibrated at higher P, suggest more oxidized conditions than in a low-P assemblage.

In this calculation, we assume that the mineral assemblage recorded the equilibrium with the fluid at one specific P-T condition along the prograde path. Garnet in Alpine Corsica metabasalts is found uniquely in eclogite-facies rocks (Vitale Brovarone et al., 2014), and the T estimate ~500 °C obtained for the carbonate-garnet isotopic equilibrium is comparable with previous peak metamorphic conditions (~500 °C and 2.2 GPa Ravna et al., 2010; Vitale Brovarone et al., 2011b). We thus reasonably assume that garnet formation in local (meta-) stable domains occurred at or close to peak P-T metamorphic conditions, where the fluid X_{CO_2} is about 0.2–0.4 mol%, with the f_{O_2} ~FMQ + 1. The estimated X_{CO_2} at the peak conditions is reasonably consistent with the $CaCO_3$ solubility in water (~0.2 mol%, Caciagli and Manning, 2003).

When the fluid flows along a T and/or P gradient, the fluid changes its composition in response to the changes in P-T conditions, which reflects the reaction progress. For the devolatilization reaction (1), when 1 mol grossular is precipitated in the rock, 2 mol CO_2 and 2 mol H_2O are released to the fluid. For reaction (2), 1 mol grossular corresponds to 5/3 mol CO_2 and 1/3 mol H_2O. Accordingly, if the devolatilization processes were taking place in a closed system, CO_2 would be greatly enriched in the fluid with small reaction progress (Greenwood, 1975). However, if the fluid is in equilibrium with the garnet-forming matrix along the flow path, the time-integrated flux can be thus estimated based on fluid mass conservation (Baumgartner and Ferry, 1991; See Supplementary Material for details and discussions). Calculations are conducted to estimate the time-integrated fluid flux into the rock to drive the devolatilization reactions at any P-T condition along the prograde P-T path, assuming that fluid flow was predominantly vertically upward through the metabasalt unit.

The time-integrated fluid flux (m^3/m^2) and CO_2 flux (g/m^2) corresponding to garnet precipitation (1 g garnet per 1 m^3 rock) are presented in Fig. 15. At P-T conditions close to the prograde path, 1 g garnet ($X_{Grs} = 0.4$) precipitates in 1 m^3 rock in response to 0.01–0.02 m^3 H_2O-CO_2 fluid flowing through 1 m^2 into the rock. The infiltrating fluid flux contains 50–70 g/m^2 CO_2, depending on the specific reactants and P-T conditions. We do not imply that the mineral assemblages were in equilibrium with the fluid throughout the prograde metamorphism, but the flux expression above depends on the fluid compositional gradient rather than the absolute values. The simulations by Ague (1998) demonstrate that even in disequilibrium, compositional gradients approach the local equilibrium case along the majority of the flow path, so the flux estimates based on equilibrium assumption are still valid. We also note that the different P-T conditions do not cause order-of-magnitude differences in the fluid flux estimates.

If the preserved mineral compositions reflect the peak stage then, for instance, 1 g garnet product in 1 m^3 rock by local devolatilization reactions corresponds to about 0.01 m^3/m^2 fluid flux flowing through (including ~70 g/m^2 CO_2). The fluid flux is a cumulative effect of devolatilization of the whole subduction section, so it is much larger than that generated from local devolatilization reactions where garnets are formed.

The garnet amount in our samples reaches ~20 vol%. We estimate that the garnet amount produced by the reactions between carbonates, epidote/lawsonite and quartz accounts for at least 40% of total garnet (8 vol% taking 20 vol% garnet in the rock; taking Gt2 and reaction (2) as a proxy for garnet). Moreover, the remaining 12 vol% is much larger than the garnet mode in the carbonate-free metabasalts, so it is highly likely that several other carbonate-consuming reactions took place in the rock. Taking 8 and 20 vol% garnet to correspond to 3×10^5 and 7.6×10^5 g per 1 m^3 rock, respectively, yields upper and lower limits of the estimate of the fluid flux through the rock of 3×10^3 and 7.6×10^3 m^3/m^2. These values are in agreement with estimated time integrated fluid fluxes in crustal metamorphic settings, and plot transitionally between flux ranges typically recognized in dominantly pervasive (<10^3 m^3/m^2) and highly channelized (>10^4 m^3/m^2) flow systems (Ague, 2014) The values are, however, much higher than the time-integrated fluid flux proposed at the top of an oceanic slab for a vertical flow (3×10^2 m^3/m^2; Zack and John, 2007). The time-integrated fluid flux leading to the garnet precipitation carried a CO_2 flux as high as 20–50 t/m^2.

9. Discussion

9.1. Origin and significance of the carbonated metabasalts of Alpine Corsica

Considerable effort has been made to estimate the amount of carbonate incorporated in oceanic basalts and its role as a carrier of C into active subduction (Staudigel et al., 1996; Jarrard, 2003; Staudigel, 2003). The study of metamorphic rocks formed tens of Ma ago (i.e. in the Jurassic for the Corsica samples) also requires consideration of long-term variation over geological timescales (Jarrard, 2003). Gillis and Coogan (2011) reviewed data from seven DSDP/ODP drill cores, and concluded that the carbonate content of the upper 300 m of the volcanic crust is higher in the slower-spreading Atlantic (0.8–4.2 wt%) than in the Pacific (0.2–2.6 wt%) crust. In both settings, the Mesozoic crusts are 2 to 13 times richer in carbonate than the Cenozoic ones (Gillis and Coogan, 2011). The Corsican basalts originated in a Mesozoic, Tethyan ocean-continent transition zone characterized by an overall crustal architecture typical of slow-spreading oceans (Lagabrielle and Lemoine, 1997; Lagabrielle et al., 2015). Therefore, in terms of C

Please cite this article as: Brovarone, A.V., et al., Intra-slab COH fluid fluxes evidenced by fluid-mediated decarbonation of lawsonite eclogite-facies altered oceanic metabasalts, Lithos (2018), https://doi.org/10.1016/j.lithos.2018.01.028

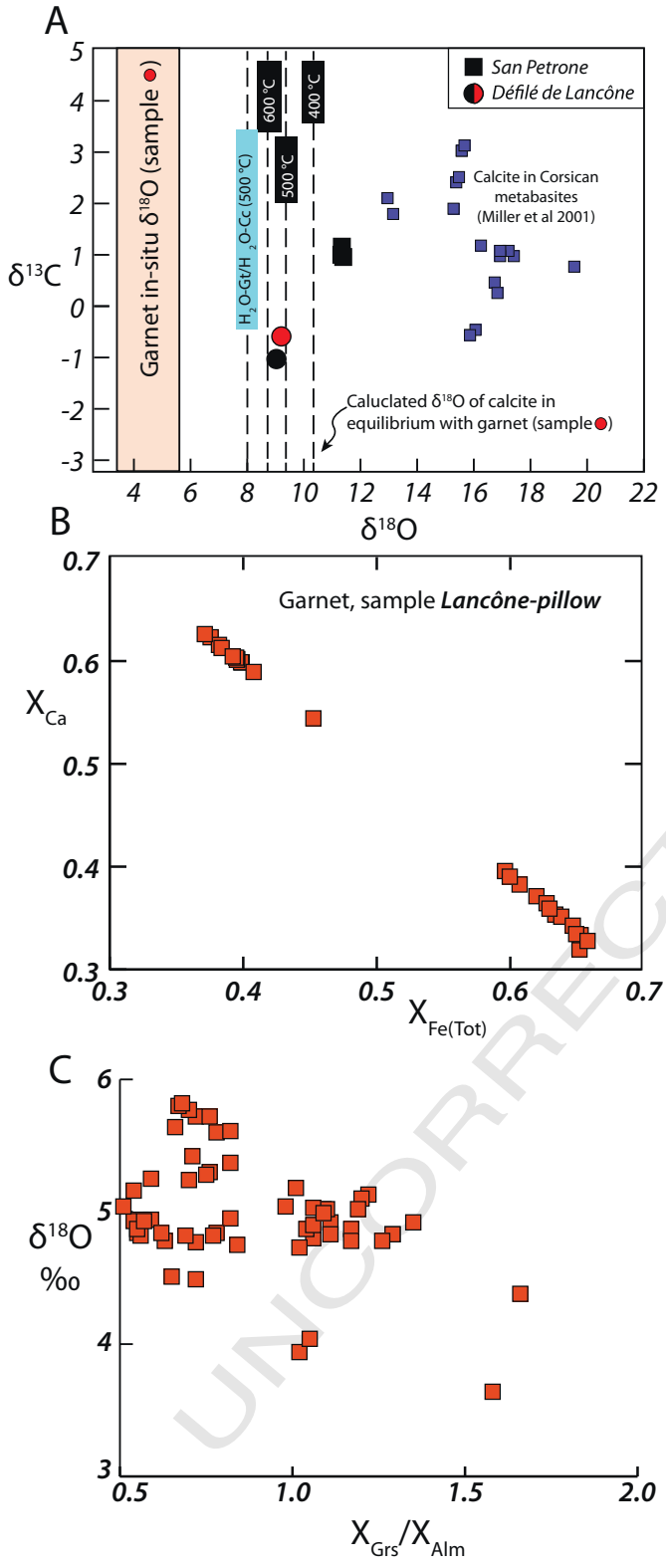

Fig. 12. (A) Diagram summarizing the whole rock carbonate ($\delta^{18}O$ and $\delta^{13}C$) and in-situ garnet ($\delta^{18}O$) stable isotope data. Previous data on eclogite-facies metabasites from Corsica are also reported (after Miller et al., 2001). The calculated $\delta^{18}O$ of calcite in equilibrium with the measured garnet values are also reported for 400, 500 and 600 °C, as well as the calculated value of H_2O in equilibrium with the measured garnet and carbonate values at 500 °C. (B) Diagram showing the bimodal zonation of Gt2 in sample Lancône-pillow alternating Ca-rich and Ca-poor zones. (C) Plot illustrating the slight inverse correlation between the Ca content in the garnet and the relative in-situ $\delta^{18}O$ values by SIMS.

content, the Corsica metabasalts can be considered as a carbonate-rich end-member.

Carbonate in oceanic basalts is mainly found in hydrothermal veins, or as disseminated material filling vesicles and intergranular void space (Alt, 1995; Alt and Teagle, 1999). Carbonate precipitation most commonly occurs in relatively LT hydrothermal veins (<100 °C). A notable exception is Hole 504B, where carbonate formed at T up to 250 °C (Alt et al., 1986; Alt and Teagle, 1999). Carbonate (dominantly calcite and minor aragonite) can also replace olivine, simultaneously precipitating phyllosilicates (e.g. saponite, celadonite) and Fe-oxyhydroxides. Carbonate is rarely found in association with epidote, the latter being formed at higher T together with quartz. Nonetheless, HT carbonate, epidote and quartz is found in Hole 504B, together with stockwork sulfide deposits. Most Corsican basalts (both weakly metamorphosed basalts and HP metabasalts) preserve seafloor hydrothermal veins showing little or no Alpine deformation. Some of these veins have features characteristic of low-T seafloor carbonate precipitation (carbonate, phyllosilicates; Fig. 4a) and their metamorphic transformations (Fig. 4B), whereas others preserve evidence for high-T seafloor hydrothermal alteration (Fig. 4C) similar to Hole 504B, such as high epidote (Ep1), quartz, carbonate, and sulfide abundances and their metamorphic transformations (Fig. 4D).

9.2. Evidence for open-system behavior at eclogite-facies conditions and infiltration of aqueous fluids

Our rocks do not show macroscopic evidence for fluid influx, e.g. outcrop-scale metasomatic halos. Despite that, the petrological observations suggest infiltration of external fluids during garnet formation during the prograde evolution. The available P-T estimates on the HP units of Alpine Corsica indicate that the prograde P-T path lies in the lawsonite stability field, where epidote should not be stable. Nevertheless, relict prograde epidote (Ep1) is widespread in our samples. Our microstructural study indicates that the conversion from Ep1 to lawsonite occurred during, or slightly before, garnet formation at eclogite-facies conditions (Fig. 13). For example, lawsonite replacing Ep1 is found as inclusions in garnet. Three main scenarios can account for the presence of epidote during the prograde evolution of our samples, (i) the presence of a high X_{CO2} fluid composition (Nitsch, 1972), (ii) insufficient water content (Ballèvre et al., 2003), and/or (iii) metastable preservation of seafloor hydrothermal epidote. The first hypothesis is unlikely in our case because titanite, which is even more sensitive to the X_{CO2} than lawsonite, was stable throughout the prograde evolution instead of rutile, as indicated by widespread titanite inclusions in garnet. The second hypothesis requires that the system was initially water-undersaturated, and the prograde, near-peak formation of lawsonite at the expense of Ep1 would therefore require significant hydration during the prograde path (Ballèvre et al., 2003; Clarke et al., 2006; Groppo et al., 2016). The third hypothesis (metastable preservation of epidote) requires overstepping of the expected lawsonite-forming reactions during the prograde path. This is not uncommon for such kinds of hydration reactions, which are expected to have low reaction affinity at low temperatures (Pattison et al., 2011; Ague and Carlson, 2013). Successive conversion of metastable epidote to lawsonite would require significant addition of water to the system, a process that is also expected to significantly lower the degree of overstepping (Pattison et al., 2011). Therefore, hypothesis (iii) also indirectly supports a fluid influx for the precipitation of lawsonite (hypothesis ii). This indicates that the prograde conversion of epidote to lawsonite resulted from hydration of undersaturated metabasalts at HP conditions, as already documented in fluid-mediated systems in Corsica and other HP belts and predicted by numerical models (Wada et al., 2012; Faccenda, 2014; Vitale Brovarone and Beyssac, 2014; Groppo et al., 2016). Interestingly, part of this newly formed lawsonite was then destabilized, with related water release, during decarbonation and garnet formation (reaction (1)) (Fig. 13). This demonstrates the

Please cite this article as: Brovarone, A.V., et al., Intra-slab COH fluid fluxes evidenced by fluid-mediated decarbonation of lawsonite eclogite-facies altered oceanic metabasalts, Lithos (2018), https://doi.org/10.1016/j.lithos.2018.01.028

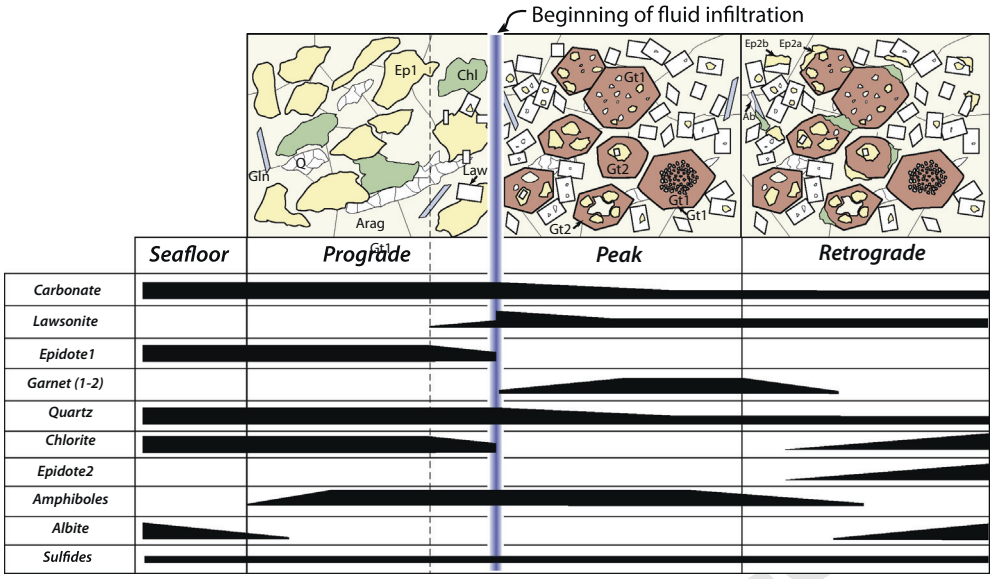

Fig. 13. Petrological evolution of sample Lancône12-6 reconstructed based on textural data. This sample shows well the complexity and diversity of the local mineral assemblages and equilibria in the studied rocks. Note that the beginning of fluid infiltration, recorded by hydration and conversion of Epidote1 to lawsonite, is followed by coupled dehydration and decarbonation processes, suggested by the consumption of lawsonite, Epidote1, carbonate and quartz to produce garnet. Abbreviations as Fig. 8.

complex role of fluid infiltration in the coupling between hydration and dehydration/decarbonation processes during the metamorphic evolution of subducting slabs.

9.3. Carbon and oxygen isotopic fingerprints of metamorphic decarbonation

Variations in $\delta^{13}C$ and $\delta^{18}O$ values for carbonate in metamorphic rocks are used as markers for decarbonation processes in subduction zones. For example, Cook-Kollars et al. (2014) and Miller et al. (2000, 2001) provided large datasets on C and O isotopic data on carbonate-bearing rocks from the Western Alps and Alpine Corsica. Both studies noticed little shift in $\delta^{13}C$ relative to the inferred marine signature (0‰), and interpreted these values as slightly affected by decarbonation or fluid-rock interactions. Nevertheless, eclogite-facies rocks affected by intense carbonate dissolution in the Syros mélange (Greece) show very little decrease in $\delta^{13}C$ relative to unaltered rocks (Ague and Nicolescu, 2014), indicating that the interpretation of $\delta^{13}C$ values of subducted carbonates in open systems requires caution. In our samples, although several mineralogical and textural pieces of evidence indicate that decarbonation reactions occurred during subduction, the carbonate $\delta^{13}C$ values do not show significant shifts relative to a reference marine carbonate source (Fig. 12A).

Our calculations show that a fairly large amount of C-bearing fluid passed through our rock to drive the inferred decarbonation reactions

Table 2.

	Lancône-pillow		Lancône12-6			Lancône12-6				Lancône12-6			Lancône12-6		OF3322	
	Gt2 Dark	Gt2 Bright	Gt1	Gt2		Ep1	Ep2 after Gt	Ep2 after Law		Blue-Amp	Green-Amp		Chl		Phe	Phe
SiO_2	37.67	36.67	37.63	38.28	SiO_2	38.52	38.66	40.38	SiO_2	57.53	57.12	SiO_2	26.83	SiO_2	53.47	53.64
Al_2O_3	18.57	20.64	21.03	20.76	Al_2O_3	27.78	26.94	30.89	Al_2O_3	10.54	7.96	Al_2O_3	19.83	Al_2O_3	23.43	23.12
TiO_2	0.01	0.11	0.12	0.18	MgO	0.02	0.00	0.02	TiO_2	0.00	0.10	MgO	23.34	TiO_2	0.07	0.13
MgO	18.49	30.07	29.20	26.40	FeO	7.38	8.14	3.34	MgO	12.85	11.91	FeO	0.29	MgO	2.99	3.07
FeO	0.06	0.52	0.54	0.44	MnO	0.11	0.03	0.24	FeO	0.00	0.14	MnO	16.77	FeO	0.02	0.02
MnO	0.00	0.07	0.53	0.39	CaO	23.57	23.58	23.24	MnO	8.83	11.31	CaO	0.06	MnO	4.64	4.68
CaO	23.95	11.69	11.38	14.08	Na_2O	0.09	0.02	0.21	CaO	0.92	4.49	Na_2O	0.10	CaO	0.06	0.05
Na_2O	0.00	0.00	0.04	0.03	K_2O	0.03	0.00	0.01	Na_2O	6.93	5.18	K_2O	0.03	Na_2O	0.12	0.09
K_2O	0.00	0.01	0.00	0.01	Cr_2O_3	0.00	0.00	0.00	K_2O	0.00	0.04	Cr_2O_3	0.00	K_2O	10.63	10.78
Cr_2O_3	0.00	0.04	0.00	0.02	Total	97.51	97.39	98.35	Cr_2O_3	0.07	0.00	Total	87.24	Total	95.43	95.59
Total	98.75	99.81	100.47	100.58					Total	97.66	98.25					
					Si	2.99	3.01	3.06				Si	5.61	Si	3.57	3.58
Si	3.00	2.96	3.00	3.03	Ti	0.00	0.00	0.00	Si	7.96	7.94	Al iv	2.39	Ti	0.00	0.01
Al iv	0.00	0.04	0.00	0.00	Al	2.55	2.47	2.76	Al iv	0.04	0.06	Al vi	2.51	Al	1.84	1.82
Al vi	1.76	1.93	1.98	1.94	Cr	0.00	0.00	0.00	Al vi	1.68	1.24	Cr	0.00	Fe^{3+}	0.00	0.00
Ti	0.00	0.01	0.01	0.01	Fe^{+3}	0.48	0.53	0.21	Ti	0.00	0.01	Fe^{3+}	0.04	Fe^{2+}	0.17	0.17
Cr	0.00	0.00	0.00	0.00	Mn	0.01	0.00	0.02	Cr	0.01	0.00	Fe^{2+}	4.04	Mn	0.00	0.00
Fe^{3+}	0.21	0.05	0.02	0.02	Mg	0.00	0.00	0.00	Fe^{3+}	0.21	0.05	Mn	0.05	Mg	0.46	0.47
Fe^{2+}	1.02	1.98	1.93	1.72	Ca	1.96	1.97	1.89	Fe^{2+}	1.27	1.33	Mg	5.23	Ca	0.00	0.00
Mn	0.00	0.04	0.04	0.03	Na	0.00	0.00	0.03	Mn	0.00	0.02	Ca	0.01	Na	0.02	0.01
Mg	0.00	0.01	0.06	0.05	K	0.00	0.00	0.00	Mg	1.82	2.34	Na	0.08	K	0.90	0.92
Ca	2.04	1.01	0.97	1.19	Total	7.99	7.99	7.97	Ca	0.14	0.67	K	0.02			
Total	9.27	8.03	8.00	7.99	XEp	0.2	0.2	0.1	Na	1.86	1.40	Oxygens	28			
XCa	0.62	0.33	0.32	0.40					K	0.00	0.01	XMg	0.56			
XMg	0.00	0.00	0.02	0.02					Oxygens	23	23					
XFe	0.38	0.66	0.65	0.58												
XMn	0.00	0.01	0.01	0.01												

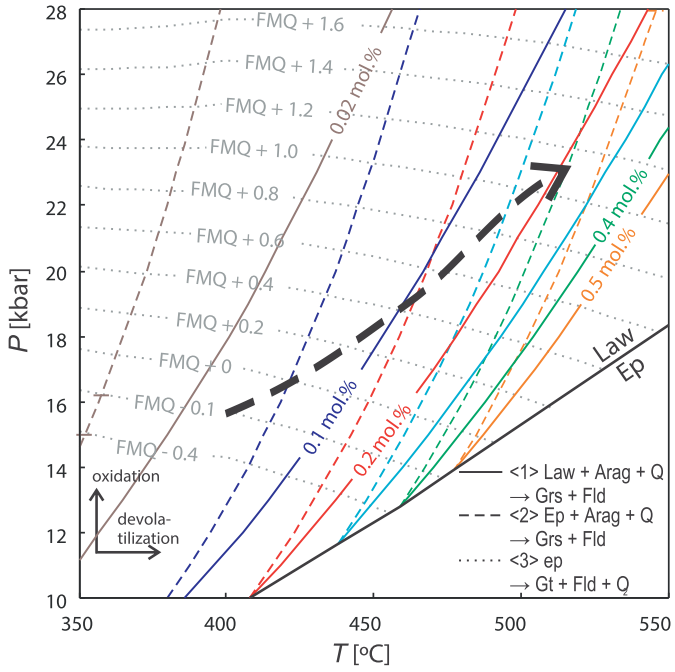

Fig. 14. Diagram illustrating the stable or metastable equilibria among lawsonite, epidote and garnet at specific X_{CO2} (mol%) and f_{O2} (relative to the FMQ buffer) in the lawsonite-bearing zone. The prograde path is superimposed for reference (after Vitale Brovarone et al., 2011a). Abbreviations: Law: lawsonite; Arag: aragonite; Q: quartz; Grs: grossular; Ep: epidote; Gt: garnet; Fld: fluid. See text for details.

(>20 t/m^2 of CO_2), suggesting that the isotopic composition of C in this fluid may have contributed to the final $\delta^{13}C$ composition of residual carbonate. If the incoming fluid was derived from dissolution of marine carbonate following the patterns observed by Ague and Nicolescu (2014), the final $\delta^{13}C$ values of the residual carbonate would not have changed significantly in the studied rocks. The $\delta^{13}C$ values of carbonate in the metamorphic crack-seals are consistent with transport of carbon preserving marine isotopic signatures. In sum, we conclude that the absence of significant shifts in $\delta^{13}C$ values does not necessarily imply that little decarbonation occurred.

The $\delta^{18}O$ values (9–11‰) of carbonate in the selected set of samples are lower than the average composition of carbonate in the Corsican metaophiolite 12–20‰, Miller et al., 2001) (Fig. 12C). Miller et al. (2001) interpreted the average values in the HP metabasaltic rocks of Corsica as evidence for the absence of large-scale, pervasive fluid flow and isotopic homogenization of the subducted altered oceanic crust. Conversely, our samples testify for isotopic equilibration at near peak conditions (see Section 6). This feature further suggests that the selected set of samples recorded channelized fluid flow enhancing isotopic equilibration of marine carbonates with silicates in the metabasaltic rocks at HP conditions. The collected in-situ $\delta^{18}O$ garnet data may constrain the timing and conditions for this equilibration. Ca-silicates resulting from decarbonation reactions in our samples are expected to inherit at least part of the $\delta^{18}O$ of the precursor carbonate, unless the rock $\delta^{18}O$ is buffered by the signature of the incoming fluid. However, if the reactant carbonate and/or the incoming fluid are equilibrated with the metabasic host rocks, the decarbonation reaction may not be obviously deduced by the $\delta^{18}O$ signature. The $\delta^{18}O$ values of Ca-rich garnet formed through decarbonation reactions do not show any significant shift relative to the Ca-poorer garnet (Fig. 13B). The absence of significant $\delta^{18}O$ variations between the garnet generations suggests that the system was buffered by an external fluid source rather than by local "closed" equilibria. The latter hypothesis would suggest that the infiltrating fluid had a $\delta^{18}O$ signature equilibrated with the metabasaltic sequence (6–11‰) in the Défilé de Lancône, (Miller et al., 2001). The $\delta^{18}O$ composition of carbonate in the metamorphic veins (about 11‰) supports this hypothesis.

Table 3

	d13C PDB	d18O SMOW
2COR12-11	1.0	11.4
OF3322	1.2	11.4
2COR12-8	1.0	11.4
Lancône-pillow	−0.6	9.1

9.4. Role of inherited seafloor hydrothermal structures on devolatilization and C circulation in subduction zones

The modes of carbonation and the spatial distribution of carbonate in the rock require additional discussion. Carbonate incorporation in the oceanic crust can be strongly inhomogeneous and localized (see Section 9.1). Owing to the complexity and variability of alteration patterns, global budgets do not account for the spatial distribution of the carbonates at the meso and microscale. Most thermodynamic studies investigating the general decarbonation patterns of oceanic subduction consider averaged oceanic basalt compositions (e.g. "Supercomposite" bulk composition of Staudigel et al., 1989) that cannot reproduce this variability. The choice of using an average composition is valid in the case of decarbonation reactions that do not directly correlate to the amount of carbonate in the rock, but may result in significant underestimations of the total produced C fluxes if carbonate dissolution is also relevant. As an example, decarbonation can be limited in carbonate-rich systems poor in silicates (Kerrick and Connolly, 2001; Gorman et al., 2006; Cook-Kollars et al., 2014). Carbonate-rich, silicate-poor hydrothermal veins may undergo little decarbonation compared to mixed carbonate-silicate assemblages, as also suggested by our data; conversely, fluid channelization along veins may potentially cause total carbonate dissolution (Ague and Nicolescu, 2014). Therefore, inherited hydrothermal systems may exert a chemical/structural feedback on C release in subduction zones.

The collected data show that large-scale chemical homogenization of subducted oceanic metabasalts is not necessarily achieved at forearc depths (see also conclusions by Miller et al., 2001), thus preserving localized domains containing carbonate amounts several times higher than the averaged compositions of altered oceanic basalts. This preservation is not only characteristic of the lawsonite-eclogites of Corsica, but is also observed in the blueschist- and eclogite-facies rocks from the Western Alps and other orogenic belts (Collins et al., 2015). Therefore, our samples can provide important insights on the potential role of structural inheritance on the patterns of C loss from subducted metabasalts.

Inherited hydrothermal vein networks are structures that may favor fluid channelization and fluid-rock interactions during subduction, as summarized in Fig. 16. The studied samples from Corsica provide the first natural evidence for such an effect, as demonstrated by the documented fluid-mediated isotopic reset, the coupled hydration-decarbonation reactions, and the estimated time-integrated fluid fluxes testifying for channelized fluid flow (see Section 8).

The composition (mineralogical and chemical) of the inherited hydrothermal material also plays an important role on the patterns of C release during subduction. The particular Ca-Al-Si-C-rich (and Fe-Mg poor) compositions (high initial carbonate, epidote, quartz) of the inherited hydrothermal veins may also be an important factor favoring decarbonation reactions that have been shown to be hampered in standard metabasaltic compositions where carbonate phases other than Ca carbonate are present (Kerrick and Connolly, 2001; Poli et al., 2009). The Fe-Mg-poor assemblages of the Corsica rocks play a key role in the development of the proposed decarbonation reactions. These particular bulk-rock compositions (together with other parameters such as f_{O2}) are probably responsible for the absence of Mg-Fe carbonates in our high-pressure assemblages, and may also have a

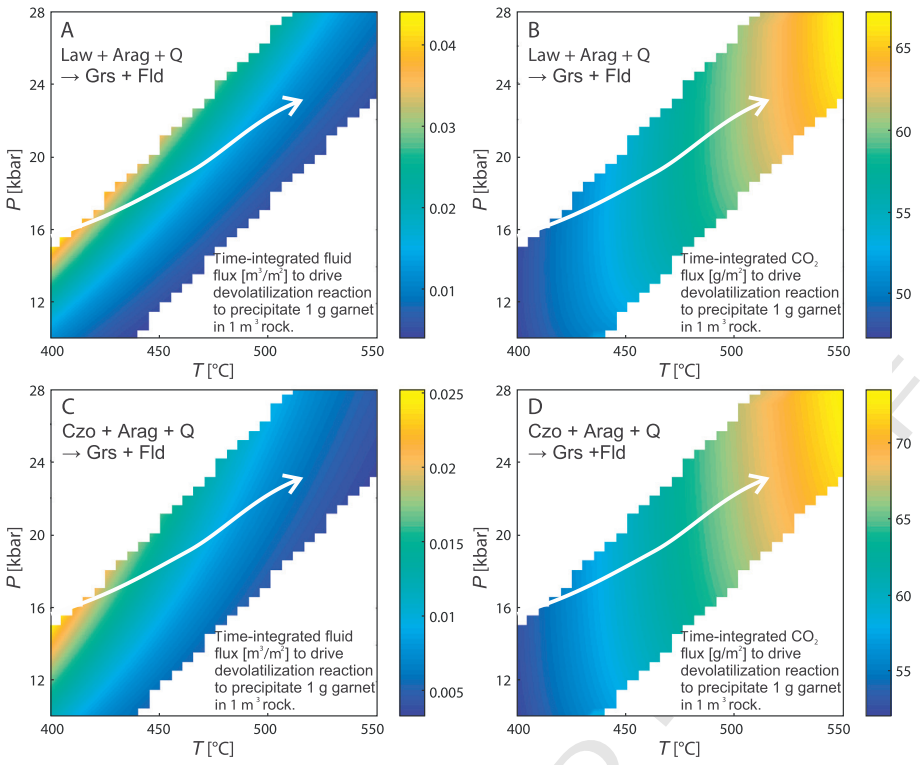

Fig. 15. Calculated time-integrated fluid flux (m^3/m^2, A, C) and CO_2 flux (g/m^2, B, D) to precipitate 1 g garnet by devolatilization reactions between aragonite, quartz and lawsonite (reaction (1), A, B) or epidote (reaction (2), C, D). The prograde path is superimposed for reference (after Vitale Brovarone et al., 2011a). Abbreviations as Fig. 14.

potential role in generating Ca-rich carbonic melts at higher P-T conditions (Poli et al., 2009; Li et al., 2014; Poli, 2015).

Moreover, the chemical/mineralogical composition of these veins may exert a positive feedback on permeability, fluid channelization and decarbonation. Wark and Watson (2002) demonstrated experimentally that the mineral assemblage strongly controls grain-scale pore channelization in systems controlled by T or compositional gradients. They showed that calcite-quartz-wollastonite rock is much more suitable for channelization than rock composed of calcite alone. This channelization effect is also documented in natural HP fluid-mediated systems (Molina et al., 2004). Nevertheless, in our rocks, decarbonation is particularly efficient in inherited hydrothermal veins containing initial carbonate, quartz and epidote, whereas it seems to be less marked in veins consisting dominantly of carbonate

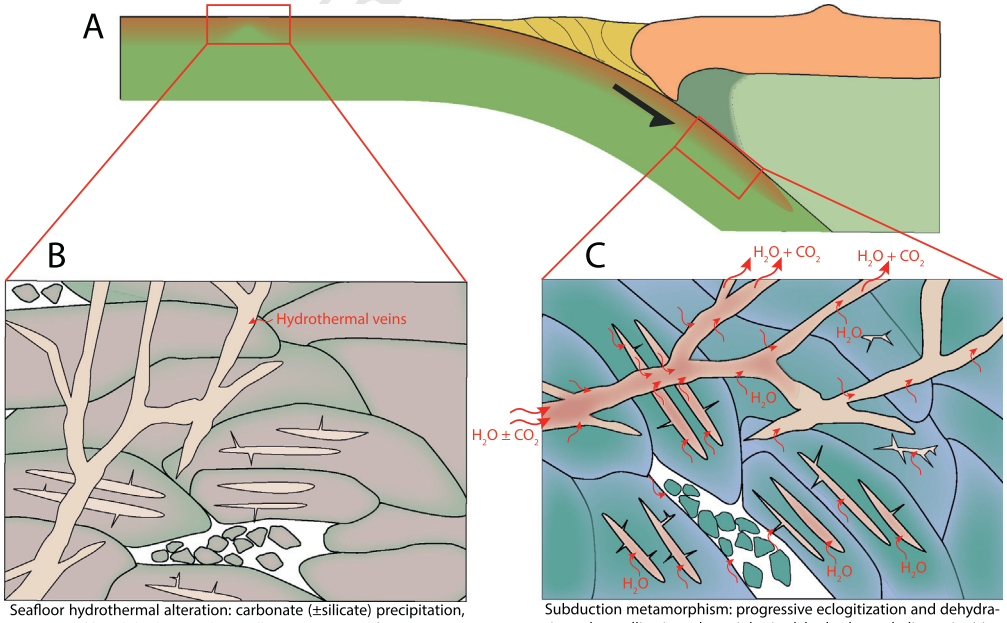

Fig. 16. (A) Schematic representation of an oceanic subduction setting showing the position of basalts emplaced and hydrothermally altered at the ridge (B) and then successively subducted to high-pressure conditions (C). The scheme is not intended to fully represent the Corsica case study, but to help the reader following the structural inheritance from (B) to (C), and its role on fluid channelization and fluid-mediated decarbonation of oceanic hydrothermal carbonates during eclogitization and dehydration at high-pressure conditions.

Please cite this article as: Brovarone, A.V., et al., Intra-slab COH fluid fluxes evidenced by fluid-mediated decarbonation of lawsonite eclogite-facies altered oceanic metabasalts, Lithos (2018), https://doi.org/10.1016/j.lithos.2018.01.028

(Supplementary material). This may be due to the interplay between mineralogical/permeability factors (Wark and Watson, 2002), even though this effect can be hampered by the progression of the decarbonation reactions (Balashov and Yardley, 1998). Last, fluid channelization along inherited hydrothermal systems can mobilize elements hosted in typical oceanic hydrothermal deposits, such as S and metals. Although our study did not focus on these elements, the studied samples contain possible evidence for transformation of sulfide deposits in the subducted metabasaltic suite (Figs. 4D, 6C).

9.5. Implications for deep C fluxes at subduction zones

Our study reports the first example of decarbonation reactions driven by fluid infiltration in a subducted segment of oceanic crust. The overall setting and field relations are consistent with the model of simple vertical fluid flow. Considering a standard geothermal model for the Corsica subduction (T increasing from the inner slab towards the overlying mantle wedge), this setting corresponds to decarbonation driven by an upward, up-T fluid flow. The cumulative time-integrated fluid flux passing through the rock and leading to the garnet precipitation carried a CO_2 flux as high as 20–50 t/m^2 (0.5–1.1 Mmol/m^2). For comparison, decarbonation induced by the interaction between this fluid and the carbonate-bearing metabasalts would release 20–60 kg CO_2 from 1 m^3 rock considering reaction (1) or (2). The lower limit is close to the infiltration-driven decarbonation model of Gorman et al. (2006) (~0.5 wt% CO_2, corresponding to 17 kg CO_2 from 1 m^3 rock).

In the Corsican slab, the basaltic section was thinner than 500 m, as indicated by lithostratigraphic observations in both low-grade units and their higher-grade equivalents (Miller et al., 2001; Vitale Brovarone et al., 2011a); a column of 500 m of such rock only releases 10–30 t/m^2 CO_2. The deficiency of CO_2 flux suggests that the majority of CO_2 flux must be derived from deeper units of the subducting slab. The studied sequence consists of basal serpentinites (±metagabbro pods), metabasalts and metasedimentary cover rocks. Although the metasedimentary cover is locally thick (>200 m) in this sequence, previous tectonostratigraphic reconstructions suggest that the polarity of the studied unit was upright during subduction and was only later affected by large-scale folding and overturning during exhumation (Vitale Brovarone et al., 2013). Therefore, it can be assumed that the primary cover of this piece of subducted oceanic lithosphere did not contribute to these fluxes, and that the extra fluxes infiltrating the metabasaltic sequence were mainly contributed by the underlying serpentinites, in line with the measured garnet and carbonate isotopic signature. Alternatively, or in addition, if the documented fluid-rock interactions occurred after the detachment of the eclogite units along the plate interface, any other underlying subducting rocks (metasediments, metaigneous, serpentinites) may have contributed to these fluxes.

The peak pressure (2.2–2.3 GPa) roughly corresponds to the forearc depth of the fluid flux pulse from the subducting slab (Gorman et al., 2006). We compare our results with those predicted by the model of Gorman et al. (2006) at the same depths. For that, we calculated a hypothetical subduction rate for Corsica by using the available constraints on the age of blueschist-facies (37 Ma; 1.8 GPa) and eclogite-facies (34 Ma; 2.3 GPa) metamorphism (Martin et al., 2011; Vitale Brovarone and Herwartz, 2013). Taking a hypothetical dip of 45°, this gives subduction rates on the order of 0.7–0.8 cm/yr. These values are similar to the estimates for the HP units of the Western Alps (>0.7 cm/yr) (Rubatto et al., 1999). Assuming an ultra-slow subduction rate 0.8 cm/yr, the time-integrated CO_2 flux can be converted to 4–9 Mmol/yr per kilometer of arc length. These values are comparable to the cumulative predictions from phase equilibria analysis for cool subduction zones by Gorman et al. (2006) (≤3 Mmol/yr for the distillation decarbonation model and ≤13 Mmol/yr for the infiltration decarbonation model). However, we note that the thickness of metabasalt in the Corsican slab (≤500 m) is thinner than the model in Gorman et al. (2006) (2 km). Moreover, the carbonate-bearing marine sediment contributes more than half of the cumulative carbon flux in Gorman et al.'s (2006) infiltration model, but such a layer is commonly thin or absent on the top of Corsica units. Thus, the general model of Gorman et al. (2006) cannot be directly applied to the Corsican study. If the contributions from the marine sediments and more than half of the metabasalt are removed from Gorman et al.'s (2006) model, the predicted cumulative time-integrated fluid flux would be significantly smaller in the infiltration decarbonation model. Thus, the order-of-magnitude estimates from natural observations in this study indicate that the decarbonation process in the subducting slab could be more intense than predicted by the conventional model. In addition to the decarbonation reactions in the basalt-sediment units (Gorman et al. 2006), other sources like the underlying mafic-ultramafic units and/or underlying subducting rocks, and other mechanisms including carbonate dissolution account for a large proportion of the total CO_2 fluxes from the slab.

9.6. Fate and residence time of carbonate in the fluid

Our data and estimates indicate that a large amount of carbonate-bearing fluid flowed during eclogite-facies metamorphism of Alpine Corsica. A proportion of these fluids may have reprecipitated carbonate minerals and other minerals at HP conditions (Piccoli et al., 2016) or have been consumed in retrograde reactions, whereas the rest was ultimately released to shallower reservoirs (Kelemen and Manning, 2015). The carbonate-bearing metamorphic crack-seals represent direct evidence for the reprecipitation of C-bearing fluids at HP conditions. The Ar-Ar dates of phengite from the carbonate-bearing eclogitic crack-seals yield minimum ages of about 29 Ma for this precipitation. This age is about 5 Ma younger than the eclogite-facies metamorphic peak for these rocks (34 Ma). Interestingly, eclogite veins from New Caledonia have been recently shown to have formed about 6 Ma later than the regional peak metamorphic conditions, and under very fast precipitation conditions (Taetz et al., 2018). These similar patterns suggest similar subduction/exhumation rates for the two fossil subduction systems and a common mechanism of fluid circulation and vein formation during the early decompression history of HP rocks. Furthermore, one of the two Corsica samples yields much younger ages of about 25 Ma (about 9 Ma younger than the age of peak metamorphism). This suggests that the C-bearing fluid remained within the slab for a long time span, although the peak metamorphic T of the rocks slightly exceeds the expected closure T for Ar-Ar (ca. 450 °C). Even though these veins contain very well preserved HP assemblages and mineral composition, the dates possibly represent the cooling ages rather than the crystallization ages. Nevertheless, these crack-seals contain typical HP assemblages, demonstrating that the reprecipitation of carbonates occurred at metamorphic conditions close the reconstructed decarbonation/dissolution processes. Other evidence for metamorphic reprecipitation of carbonate has been documented in Corsica. Intense metamorphic carbonation has been recently reported in the eclogitic units of Corsica in rocks of the metabasaltic suite (Piccoli et al., 2016), and may possibly testify for the migration of these carbonic fluids within the slab.

Experimental studies (Caciagli and Manning, 2003) and field observations (Ague and Nicolescu, 2014) indicate that carbonate dissolves in water congruently. In our case, this would imply that a fair amount of Ca is also released from pillow basalts during metamorphism and can interact with the surrounding lithologies. Part of this Ca was bound in silicates such as the newly-formed garnet.

10. Conclusion

Dehydration, decarbonation and carbonate dissolution accompany subduction of oceanic crustal sequences and release large amounts of C-O-H-bearing fluids. The exceptional lawsonite-eclogite facies rocks of Corsica provide insights into the interplay between these processes and their contributions to the C budget in subducting slabs. The studied

Please cite this article as: Brovarone, A.V., et al., Intra-slab COH fluid fluxes evidenced by fluid-mediated decarbonation of lawsonite eclogite-facies altered oceanic metabasalts, Lithos (2018), https://doi.org/10.1016/j.lithos.2018.01.028

samples indicate that structures and mineral assemblages inherited from seafloor hydrothermal alteration play an important role in the localization of important fluid-rock processes at HP conditions. Primary hydrothermal structures concentrating high amounts of carbonates may act as the preferential sites for fluid localization and fluid-rock interactions. Our data indicate that coupled hydration and decarbonation/dehydration processes driven by upward, up-T fluid flow are responsible for the release of significant amounts of carbonic fluids during prograde metamorphism. The calculated amount of CO_2 released by these reactions in the natural samples (20–70 kg per m^3 of reacted rock) is consistent with (or higher than) the estimates for decarbonation of metabasalts under open system behavior at comparable depths (17 kg per m^3). Conversely, the calculated time-integrated CO_2 fluxes through the upper part of the subducted oceanic crust are potentially much greater than previously proposed cumulative fluxes that are generated throughout slab sections. The Corsican rocks indicate that only a portion of these fluids was released from the slab, whereas the rest was involved in successive intra-slab fluid-rock interactions leading to partial carbonate precipitation and decrease of dissolved carbon. Further effort will be necessary to integrate these data into a coherent model of fluid flow and fluxes through a complete section of subducting oceanic lithosphere.

Supplementary data to this article can be found online at https://doi.org/10.1016/j.lithos.2018.01.028.

Acknowledgements

Q26 We thank DCO Reservoirs & Fluxes and ATM-MNHN for financial support of this project. Jeff Alt is thanked for inspiring discussions on the patterns of alteration of oceanic basalts. Stefano Poli and Jodie Miller are thanked for their reviews on this work, including very constructive and frank comments. Marco Scambelluri is thanked for editorial handling. Michel Fialin and Nicolas Rividi are thanked for technical assistance at Service Camparis. AVB thanks Paulette and Jean-Paul Santori for all the nice moments spent together since 2006. The authors acknowledge the facilities and the scientific and technical assistance of the Australian Microscopy & Microanalysis Research Facility at the Centre for Microscopy, Characterisation & Analysis, The University of Western Australia, a facility funded by the University, State and Commonwealth Governments.

References

Ague, J.J., 1998. Simple models of coupled fluid infiltration and redox reactions in the crust. Contributions to Mineralogy and Petrology 132, 180–197.
Ague, J.J., 2014. Fluid flow in the deep crust. In: Holland, H.D., Turekian, K.K. (Eds.), Treatise on Geochemistry. Geological Society of America, pp. 203–247.
Ague, J.J., Carlson, W.D., 2013. Metamorphism as garnet sees it: the kinetics of nucleation and growth, equilibration, and diffusional relaxation. Elements 9, 439–445.
Ague, J.J., Nicolescu, S., 2014. Carbon dioxide released from subduction zones by fluid-mediated reactions. Nature Geoscience 7, 355–360.
Alt, J.C., 1995. Subseafloor Processes in Mid-Ocean Ridge Hydrothermal Systems, Das P-T-X_{CO2} Stabilitätsfeld Von Lawsonit. American Geophysical Union, Washington, DC.
Q27 Alt, J.C., Teagle, D., 1999. The uptake of carbon during alteration of ocean crust. Geochimica et Cosmochimica Acta.
Q28 Alt, J.C., Muehlenbachs, K., Honnorez, J., 1986. An oxygen isotopic profile through the upper kilometer of the oceanic crust, DSDP Hole 504B. Earth and Planetary Science Letters.
Balashov, V.N., Yardley, B., 1998. Modeling metamorphic fluid flow with reaction-compaction permeability feedbacks. American Journal of Science 298, 441–470.
Q29 Ballèvre, M., Pitra, P., Bohn, M., 2003. Lawsonite growth in the epidote blueschists from the Ile de Groix (Armorican Massif, France): a potential geobarometer. Journal of Metamorphic Geology.
Baumgartner, L.P., Ferry, J.M., 1991. A model for coupled fluid-flow and mixed-volatile mineral reactions with applications to regional metamorphism. Contributions to Mineralogy and Petrology 106, 270–285.
Beltrando, M., Manatschal, G., Mohn, G., Dal Piaz, G., Vitale Brovarone, A., Masini, E., 2014. Recognizing remnants of magma-poor rifted margins in high-pressure orogenic belts: the Alpine case study. Earth Science Reviews 131, 88–115.
Brunet, C., Monié, P., Jolivet, L., Cadet, J.P., 2000. Migration of compression and extension in the Tyrrhenian Sea, insights from $^{40}Ar/^{39}Ar$ ages on micas along a transect from Corsica to Tuscany. Tectonophysics 321, 127–155.
Caron, J.M., Delcey, R., 1979. Lithostratigraphie des schistes lustrés corses: diversité des séries post-ophiolitiques. Comptes Rendus de l'Académie des Sciences 208, 1525–1528.
Caron, J.M., Péquignot, G., 1986. The transition between blue-schist and lawsonite bearing eclogites on the example of Corsican metabasalt. Lithos 19, 205–218.
Chu, X., Ague, J.J., 2013. Phase equilibria for graphitic metapelite including solution of CO_2 in melt and cordierite: implications for dehydration, partial melting and graphite precipitation. Journal of Metamorphic Geology 31, 843–862.
Clarke, G.L., Powell, R., Fitzherbert, J.A., 2006. The lawsonite paradox: a comparison of field evidence and mineral equilibria modelling. Journal of Metamorphic Geology 24, 715–725.
Collins, N.C., Bebout, G.E., Angiboust, S., Agard, P., Scambelluri, M., Crispini, L., John, T., 2015. Subduction zone metamorphic pathway for deep carbon cycling: II. Evidence from HP/UHP metabasaltic rocks and ophicarbonates. Chemical Geology 412, 132–150.
Cook-Kollars, J., Bebout, G.E., Collins, N.C., Angiboust, S., 2014. Subduction zone metamorphic pathway for deep carbon cycling: I. Evidence from HP/UHP metasedimentary rocks, Italian alps. Chemical Geology. Q30
Donohue, C.L., Essene, E.J., 2000. An oxygen barometer with the assemblage garnet–epidote. Earth and Planetary Science Letters 181, 459–472.
Faccenda, M., 2014. Water in the slab: a trilogy. Tectonophysics 614, 1–30.
Ferrando, S., Groppo, C., Frezzotti, M.-L., Castelli, D., Proyer, A., 2017. Dissolving dolomite in a stable UHP mineral assemblage: evidence from Cal-Dol marbles of the Dora-Maira Massif (Italian Western Alps). American Mineralogist 102, 42–60.
Frezzotti, M.L., Selverstone, J., Sharp, Z.D., Compagnoni, R., 2011. Carbonate dissolution during subduction revealed by diamond-bearing rocks from the Alps. Nature Geoscience 4, 703–706.
Gillis, K.M., Coogan, L.A., 2011. Earth and Planetary Science Letters 302, 385–392.
Gonzalez, C.M., Gorczyk, W., Gerya, T.V., 2016. Decarbonation of subducting slabs: insight from petrological–thermomechanical modeling. Gondwana Research 36, 314–332.
Gorman, P.J., Kerrick, D.M., Connolly, J.A.D., 2006. Modeling open system metamorphic decarbonation of subducting slabs. Geochemistry, Geophysics, Geosystems 7, 1–21.
Greenwood, H.J., 1975. Buffering of pore fluids by metamorphic reactions. American Journal of Science 275, 573–593.
Groppo, C., Rolfo, F., Sachan, H.K., Rai, S.K., 2016. Petrology of blueschist from the Western Himalaya (Ladakh, NW India): exploring the complex behavior of a lawsonite-bearing system in a paleo-accretionary setting. Lithos 252-253, 41–56.
Guevara, V.E., Caddick, M.J., 2016. Shooting at a moving target: phase equilibria modelling of high-temperature metamorphism. Journal of Metamorphic Geology 34, 209–235.
Hammouda, T., 2003. High-pressure melting of carbonated eclogite and experimental constraints on carbon recycling and storage in the mantle. Earth and Planetary Science Letters 214, 357–368.
Healy, D., Reddy, S.M., Timms, N.E., Gray, E.M., Vitale Brovarone, A., 2009. Earth and Planetary Science Letters 283, 75–86.
Holland, T.J.B., Powell, R., 1998. An internally consistent interest, thermodynamic data set for phases of petrological interest. Journal of Metamorphic Geology 16, 309–343. Q31
Holland, T.J.B., Powell, R., 2003. Activity-composition relations for phases in petrological calculations: an asymmetric multicomponent formulation. Contributions to Mineralogy and Petrology 145, 492–501.
Jarrard, R.D., 2003. Subduction fluxes of water, carbon dioxide, chlorine, and potassium. Geochemistry, Geophysics, Geosystems 4.
Jolivet, L., Faccenna, C., Goff, E.B., Mattei, M., Rossetti, F., Brunet, C., Storti, F., Funiciello, R., Cadet, P., Agostino, N., Parra, T., 1998. Midcrustal shear zones in postorogenic extension: example from the northern Tyrrhenian Sea. Journal of Geochemical Exploration 103.
Kelemen, P.B., Manning, C.E., 2015. Reevaluating carbon fluxes in subduction zones, what goes down, mostly comes up. Presented at the Proceedings of the National Academy of Sciences.
Kerrick, D.M., Connolly, J.A.D., 2001. Metamorphic devolatilization of subducted oceanic metabasalts: implications for seismicity, arc magmatism and volatile recycling. Earth and Planetary Science Letters 189, 19–29.
Keshav, S., Gudfinnsson, G.H., 2010. Experimentally dictated stability of carbonated oceanic crust to moderately great depths in the Earth: results from the solidus determination in the system CaO-MgO-Al_2O_3-SiO_2-CO_2. Journal of Geophysical Research 115, B05205.
Lagabrielle, Y., Lemoine, M., 1997. Alpine, Corsican and Apennine ophiolites: the slow-spreading ridge model. Comptes Rendus de l"Acad"emie des Sciences 325, 909–920.
Lagabrielle, Y., Vitale Brovarone, A., Ildefonse, B., 2015. Earth-science reviews. Earth Science Reviews 141, 1–26. Q32
Lahondère, D., Guerrot, C., 1997. Datation Nd-Sm du métamorphisme éclogitique en Corse alpine: un argument pour l"existence, au Crétacé supérieur, d"une zone de subduction active localisée le long du block corse-sarde. Géologie de la France 3, 3–11.
Li, J.L., Klemd, R., Gao, J., Meyer, M., 2012. Coexisting carbonate-bearing eclogite and blueschist in SW Tianshan, China: petrology and phase equilibria. Journal of Asian Earth Sciences 60, 174–187.
Li, J.L., Klemd, R., Gao, J., Meyer, M., 2014. Compositional zoning in dolomite from lawsonite-bearing eclogite (SW Tianshan, China): evidence for prograde metamorphism during subduction of oceanic crust. American Mineralogist 99, 206–217.
Malavieille, J., Chemenda, A., Larroque, C., 1998. Evolutionary model for Alpine Corsica: mechanism for ophiolite emplacement and exhumation of high-pressure rocks. Terra Nova 10, 317–322.
Malusà, M.G., Faccenna, C., Baldwin, S.L., Fitzgerald, P.G., Rossetti, F., Balestrieri, M.L., Danišík, M., Ellero, A., Ottria, G., Piromallo, C., 2015. Contrasting styles of (U)HP rock exhumation along the Cenozoic Adria-Europe plate boundary (Western Alps, Calabria, Corsica). Geochemistry, Geophysics, Geosystems 16, 1786–1824.
Marroni, M., Pandolfi, L., 2003. Deformation history of the ophiolite sequence from the Balagne Nappe, northern Corsica: insights in the tectonic evolution of Alpine Corsica. Geological Journal 38, 67–83.
Martin, L.A.J., Rubatto, D., Vitale Brovarone, A., Hermann, J., 2011. Late Eocene lawsonite-eclogite facies metasomatism of a granulite sliver associated to ophiolites in Alpine Corsica. Lithos 125, 620–640.

Please cite this article as: Brovarone, A.V., et al., Intra-slab COH fluid fluxes evidenced by fluid-mediated decarbonation of lawsonite eclogite-facies altered oceanic metabasalts, Lithos (2018), https://doi.org/10.1016/j.lithos.2018.01.028

Meresse, F., Lagabrielle, Y., Malavieille, J., Ildefonse, B., 2012. Tectonophysics. Tectonophysics 579, 4–16.
Miller, J.A., Cartwright, I., 2006. Albite vein formation during exhumation of high-pressure terranes: a case study from alpine Corsica. Journal of Metamorphic Geology 24, 409–428.
Miller, J.A., Buick, I.S., Cartwright, I., 2000. Textural implications of high-pressure fluid flow controlled by pre-subduction deformation and alteration patterns. Journal of Geochemical Exploration 69-70, 551–555.
Miller, J.A., Cartwright, I., Buick, I.S., Barnicoat, A.C., 2001. An O-isotope profile through the HP–LT Corsican ophiolite, France and its implications for fluid flow during subduction. Chemical Geology 178, 43–69.
Molina, J.F., Poli, S., Austrheim, H.K., Glodny, J., Rusin, A., 2004. Eclogite-facies vein systems in the Marun-Keu complex (Polar Urals, Russia): textural, chemical and thermal constraints for patterns of fluid flow in the lower crust. Contributions to Mineralogy and Petrology 147, 484–504.
Pattison, D.R.M., de Capitani, C., GAIDIES, F., 2011. Petrological consequences of variations in metamorphic reaction affinity. Journal of Metamorphic Geology 29, 953–977.
Piccoli, F., Vitale Brovarone, A., Beyssac, O., Martinez, I., Ague, J.J., Chaduteau, C., 2016. Carbonation by fluid–rock interactions at high-pressure conditions: implications for carbon cycling in subduction zones. Earth and Planetary Science Letters 445, 146–159.
Plümper, O., John, T., Podladchikov, Y.Y., Vrijmoed, J.C., Scambelluri, M., 2016. Fluid escape from subduction zones controlled by channel-forming reactive porosity. Nature Geoscience 10, 150–156.
Poli, S., 2015. Carbon mobilized at shallow depths in subduction zones by carbonatitic liquids. Nature Geoscience 8, 633–636.
Poli, S., Franzolin, E., Fumagalli, P., Crottini, A., 2009. The transport of carbon and hydrogen in subducted oceanic crust: an experimental study to 5 GPa. Earth and Planetary Science Letters 278, 350–360.
Ravna, E.J.K., Andersen, T.B., Jolivet, L., de Capitani, C., 2010. Cold subduction and the formation of lawsonite eclogite - constraints from prograde evolution of eclogitized pillow lava from Corsica. 28, 381–395.
Rossi, P., Cocherie, A., Lahondère, D., Fanning, C.M., 2002. La marge européenne de la Téthys jurassique en Corse: datation de trondhjémites de Balagne et indices de croûte continentale sous le domaine Balano-Ligure. Comptes Rendus Geoscience 334, 313–322.
Rubatto, D., Gebauer, D., Compagnoni, R., 1999. Dating of eclogite-facies zircons: the age of Alpine metamorphism in the Sesia–Lanzo Zone (Western Alps). Earth and Planetary Science 167, 141–158.
Scambelluri, M., Bebout, G.E., Belmonte, D., Gilio, M., Campomenosi, N., Collins, N., Crispini, L., 2016. Earth and Planetary Science Letters 441, 155–166.
Staudigel, H., 2003. Hydrothermal alteration processes in the oceanic crust. Treatise on Geochemistry 3, 511–535.
Staudigel, H., 2014. 4.16 Chemical fluxes from hydrothermal alteration of the oceanic crust. The Crust, 2nd ed. Elsevier Ltd.
Staudigel, H., Hart, S.R., Schmincke, H.U., Smith, B.M., 1989. Cretaceous ocean crust at DSDP Sites 417 and 418: carbon uptake from weathering versus loss by magmatic outgassing. Geochimica et Cosmochimica Acta 53, 3091–3094.
Staudigel, H., Plank, T., White, W.M., Schmincke, H.U., 1996. Geochemical fluxes during seafloor alteration of the upper oceanic crust: DSDP Sites 417 and 418. In: Bebout, G.E., Scholl, D.W., Kirby, S.H., Platt, J.P. (Eds.), SUBCON: Subduction From Top to Bottom. AGU Geophysical Monograph, pp. 19–38.
Stüwe, K., 1997. Effective bulk composition changes due to cooling: a model predicting complexities in retrograde reaction textures. Contributions to Mineralogy and Petrology 129, 43–52.
Syracuse, E.M., van Keken, P.E., Abers, G.A., 2010. The global range of subduction zone thermal models. Physics of the Earth and Planetary Interiors 183, 73–90.
Taetz, S., John, T., Bröcker, M., Spandler, C., Stracke, A., 2018. Fast intraslab fluid-flow events linked to pulses of high pore fluid pressure at the subducted plate interface. Earth and Planetary Science Letters 482, 33–43.
Tsujimori, T., Ernst, W.G., 2014. Lawsonite blueschists and lawsonite eclogites as proxies for palaeo-subduction zone processes: a review. Journal of Metamorphic Geology 32, 437–454.
van Keken, P.E., Hacker, B.R., Syracuse, E.M., Abers, G.A., 2011. Subduction factory: 4. Depth-dependent flux of H_2O from subducting slabs worldwide. Journal of Geophysical Research 116, B01401.
Vitale Brovarone, A., Beyssac, O., 2014. Lawsonite metasomatism: a new route for water to the deep Earth. Earth and Planetary Science Letters 393, 275–284.
Vitale Brovarone, A., Herwartz, D., 2013. Timing of HP metamorphism in the Schistes Lustrés of Alpine Corsica: new Lu–Hf garnet and lawsonite ages. Lithos 172-173, 175–191.
Vitale Brovarone, A., Beltrando, M., Malavieille, J., Giuntoli, F., Tondella, E., Groppo, C., Beyssac, O., Compagnoni, R., 2011a. Inherited Ocean–Continent Transition zones in deeply subducted terranes: insights from Alpine Corsica. Lithos 124, 273–290.
Vitale Brovarone, A., Groppo, C., Hetényi, G., Compagnoni, R., Malavieille, J., 2011b. Coexistence of lawsonite-bearing eclogite and blueschist: phase equilibria modelling of Alpine Corsica metabasalts and petrological evolution of subducting slabs. Journal of Metamorphic Geology 29, 583–600.
Vitale Brovarone, A., Beyssac, O., Malavieille, J., Molli, G., Beltrando, M., Compagnoni, R., 2013. Stacking and metamorphism of continuous segments of subducted lithosphere in a high-pressure wedge: the example of Alpine Corsica (France). Earth Science Reviews 116, 35–56.
Vitale Brovarone, A., Picatto, M., Beyssac, O., Lagabrielle, Y., 2014. The blueschist–eclogite transition in the Alpine chain: P–T paths and the role of slow-spreading extensional structures in the evolution of HP–LT mountain belts. Tectonophysics 615-616, 96–121.
Wada, I., Behn, M.D., Shaw, A.M., 2012. Earth and Planetary Science Letters 353-354, 60–71.
Wark, D.A., Watson, B., 2002. Grain-scale channelization of pores due to gradients in temperature or composition of intergranular fluid or melt. Journal of Geophysical Research 107 (5–1–15).
White, R.W., Powell, R., Holland, T.J.B., 2007. Progress relating to calculation of partial melting equilibria for metapelites. Journal of Metamorphic Geology 25, 511–527.
Zack, T., John, T., 2007. An evaluation of reactive fluid flow and trace element mobility in subducting slabs. Chemical Geology 239, 199–216.

Please cite this article as: Brovarone, A.V., et al., Intra-slab COH fluid fluxes evidenced by fluid-mediated decarbonation of lawsonite eclogite-facies altered oceanic metabasalts, Lithos (2018), https://doi.org/10.1016/j.lithos.2018.01.028